Inorganic Chemistry

pubs.acs.org/IC

Article

Isolable Coinage Metal Propylene Complexes and Trigonal Pyramids with Tris(pyridyl)borate Ligands

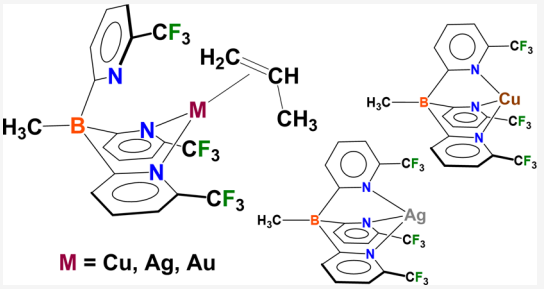
Vo Quang Huy Phan, Mukundam Vanga, Alvaro Muñoz-Castro,* Sayan Maiti, Shengqian Ma,* and H. V. Rasika Dias*

Cite This: *Inorg. Chem.* 2026, 65, 14287−14300

Read Online

ACCESS | Metrics & More | Article Recommendations | Supporting Information

ABSTRACT: The fluorinated tris(pyridyl)borate ligand $[MeB(6\text{-}(CF_3)\text{-}Py)_3]^-$ provides access to a series of isoleptic, coinage-metal propylene complexes, $[MeB(6\text{-}(CF_3)Py_3]M(C_3H_6)$ (M = Cu, Ag, Au), which were isolated and thoroughly characterized. Tris(pyridyl)borate coordinates to metal ions in a κ^2-fashion. The copper(I) and silver(I) derivatives exhibit reversible propylene binding, and loss of the olefin affords the propylene-free species $[MeB(6\text{-}(CF_3)Py)_3]M$ (M = Cu, Ag), featuring three-coordinate, trigonal pyramidal metal sites. Theoretical studies of $[MeB(6\text{-}(CF_3)Py_3]M\text{-}(C_3H_6)$ show that the metal−propylene interaction is strongest in gold(I), followed by copper(I) and silver(I), with bonding involving significant metal-to-alkene π-backdonation, which is relatively stronger than alkene-to-metal σ-donation in all three complexes. The electrostatic component in metal−propylene interaction in these complexes is quite strong. Solid-state structural data and solution NMR data of $[MeB(6\text{-}(CF_3)Py_3]M(C_3H_6)$ are consistent with these inferences. Gas adsorption studies of solid $[MeB(6\text{-}(CF_3)Py)_3]M$ (M = Cu, Ag) show a higher uptake of propane than propylene, indicating that host−guest interactions within the fluorinated ligand environment play a dominant role in the adsorption behavior. Aziridination studies demonstrate that the copper complex is effective in nitrene transfer reactions to alkenes, highlighting the potential of fluorinated poly(pyridyl)borate ligand supports in catalysis applications.



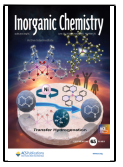
INTRODUCTION

Propylene (C_3H_6) is a vital feedstock in the chemical industry, used as a raw material for key products like polypropylene, propylene oxide, acrylonitrile, and cumene.[1,2] Coinage metals (Cu, Ag, Au)[3] play an important role in some of these and other transformations involving propylene, as well as in processes that produce propylene. For example, gold is among the most effective catalysts for the partial oxidation of propylene, yielding propylene oxide.[4−7] Silver and copper catalysts are also known to mediate this process quite effectively.[8−12] Copper-mediated electrochemical synthesis of propylene from CO_2[13] and the dehydrogenation of propane to afford propylene,[14−17] propylene transformation to arenes and acrolein[18,19] have also been reported. In addition, silver-mediated propylene electro-oxidation to propylene glycol,[20] gold-mediated oxidation of propylene to acrolein,[21] the hydroamination chemistry of propylene,[22] etc., are known.

Furthermore, alternative, energy-efficient methods for separating propylene from propane, which is a common byproduct of propylene manufacturing, are of current interest,[23−25] with adsorptive separation methods that rely on selective π-complexation of the propylene being particularly attractive for this goal.[26−28] Copper- and silver-based molecules and materials show high promise in these applications.[26,29−35] Coinage-metal propylene complexes are also the focus of computational and spectroscopic studies.[36−40] Overall, copper, silver, and gold are important metals in chemical and physical processes involving propylene, and therefore, a better understanding of the nature of the propylene interaction with these metal ions is quite useful.

Interestingly, despite their significance, isolable and structurally authenticated molecules of coinage-metal propylene complexes are quite limited. For example, a search of the Cambridge Structural Database[41] of propylene complexes of Cu(I), Ag(I), and Au(I) returned just five hits (Figure 1), $[H_2B(3,5\text{-}(CF_3)_2Pz)_2]Cu(C_3H_6)$ (**1**, Pz = pyrazolyl),[29] $\{\mu\text{-}[(3,5\text{-}(CF_3)_2Pz)_2]Cu(C_3H_6)\}_2$ (with both *cis*- and *trans*-dispositions of the two propylene groups, **2**−**3**),[42] $\{\mu\text{-}[(4\text{-}Br\text{-}3,5\text{-}(CF_3)_2Pz)_2]Cu(C_3H_6)\}_2$ (**4**),[42] and $[\{(4,4'\text{-di-}t\text{-butyl}[1,1'\text{-biphenyl}]\text{-}2\text{-yl})_3P\}Au((C_3H_6)]SbF_6$ (**5**, with artificially shortened C═C distance due to disorder),[43] with no examples involving silver(I). In addition, structural studies on a metal−organic framework Cu(II)-propylene adduct $\{Cu_2[(S,S)\text{-}$

Received: April 10, 2026
Revised: May 27, 2026
Accepted: June 3, 2026
Published: June 15, 2026



© 2026 The Authors. Published by American Chemical Society

Downloaded from http://pubs.acs.org/inocaj/article-pdf/65/25/14287/6524819/acs.inorgchem.6c01837.pdf by UNIV OF NORTH TEXAS user on 28 July 2026

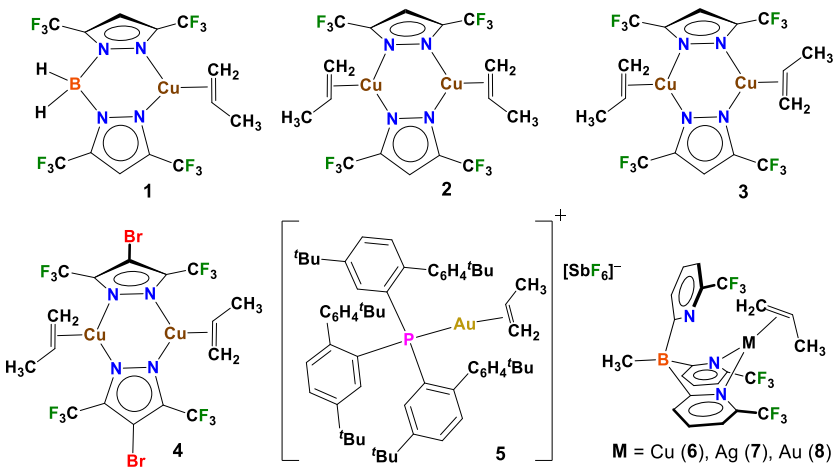


Figure 1. Isolable and structurally characterized propylene complexes of copper(I) and gold(I) in the literature and the focus of this work: [MeB(6-$(CF_3)Py)_3$]Cu(C_3H_6) (**6**), [MeB(6-$(CF_3)Py)_3$]Ag(C_3H_6) (**7**), and [MeB(6-$(CF_3)Py)_3$]Au(C_3H_6) (**8**) (Py = pyridyl).

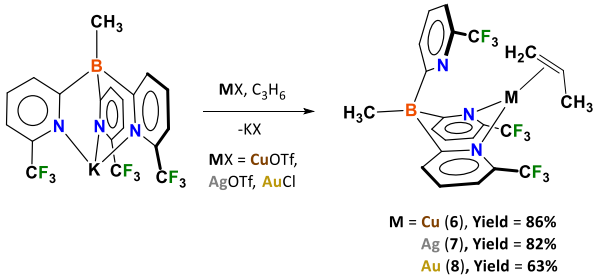
hismox]}•2C_3H_6 (hismox = bis[(*S*)-histidine]oxalyl diamide) have been reported.[44]

An area of research focus in one of our laboratories concerns the study of coinage-metal-ion complexes of industrially relevant carbon-based gaseous molecules.[45−48] Here, we present our findings on coinage-metal propylene complexes. In particular, we report the synthesis of an isoleptic series of Cu(I), Ag(I), and Au(I) propylene complexes [MeB(6-$(CF_3)Py)_3$]Cu(C_3H_6) (**6**), [MeB(6-$(CF_3)Py)_3$]Ag(C_3H_6) (**7**), and [MeB(6-$(CF_3)Py)_3$]Au(C_3H_6) (**8**) (Py = pyridyl), using a recently developed fluorinated tris(pyridyl)borate ligand, $[MeB(6\text{-}(CF_3)Py)_3]^-$,[49] including their spectroscopic, solid-state structural data, and computational analysis. We also report the isolation of rare, three-coordinate, trigonal-pyramidal copper and silver adducts.

RESULTS AND DISCUSSION

The treatment of [MeB(6-$(CF_3)Py)_3$]K[49] with the appropriate coinage metal precursors in propylene-saturated dichloromethane (Scheme 1) afforded the propylene complexes

Scheme 1. Synthesis of Coinage Metal Propylene Complexes Supported by *B*-Methylated Tris(pyridyl)borate: [MeB(6-$(CF_3)Py)_3$]Cu(C_3H_6) (6), [MeB(6-$(CF_3)Py)_3$]Ag(C_3H_6) (7), and [MeB(6-$(CF_3)Py)_3$]Au(C_3H_6) (8)



[MeB(6-$(CF_3)Py)_3$]Cu(C_3H_6) (**6**), [MeB(6-$(CF_3)Py)_3$]Ag(C_3H_6) (**7**), and [MeB(6-$(CF_3)Py)_3$]Au(C_3H_6) (**8**) as white solids in good yields. The synthesis of the gold complex required low temperatures at the initial stage of the reaction to minimize decomposition. Complex **8** retained coordinated propylene under reduced pressure and remained stable at low temperature (−20 °C) for a few days in both the solid state and in solution, although it was moisture-sensitive and formed black solids upon exposure to air. In contrast, the copper and silver propylene complexes, **6** and **7**, could only be isolated and dried under a continuous stream of propylene, as both readily lost the coordinated propylene under reduced pressure, affording propylene-free, air-and light-stable white solids. These species readily regenerate complexes **6** and **7** upon treatment of their concentrated dichloromethane solutions with propylene.

Compounds [MeB(6-$(CF_3)Py)_3$]Cu(C_3H_6) (**6**), [MeB(6-$(CF_3)Py)_3$]Ag(C_3H_6) (**7**), and [MeB(6-$(CF_3)Py)_3$]Au(C_3H_6) (**8**) were characterized by several analytical techniques, including single crystal X-ray crystallography, which revealed that propylene coordinates to the metal center in an η^2-fashion (Figure 2). These molecules feature trigonal planar, three-coordinate coinage-metal centers in which only two pyridyl arms of the tris(pyridyl)borate ligand bind to the metal (adopting a κ^2-*N,N* coordination mode), while the third pyridyl arm sits above, oriented nearly parallel to the metal−propylene plane. In all three cases, the methyl group of the coordinated propylene points outward, away from the flanking, noncoordinating pyridyl arm, to minimize steric interaction.

Unfortunately, the coordinated propylene in **6** and **7** and the gold-propylene fragment in **8** exhibit positional disorder over two sites (with % atomic occupancy of 60:40, 72:28, 58:42, respectively), arising from two orientations of the bound propylene with the methyl moiety residing on the left or right side of the N−Cu−N plane (Figure 3). Such disorder is not unusual in metal−olefin complexes and has been observed in other systems.[50−54] However, due to the two positional disorders of the propylene moiety observed in the solid-state structures, metrical parameters associated with propylene groups should be treated with due caution. Nevertheless, refinement of molecular structures proceeded well, and the data provide useful information for comparisons.

Selected average bond lengths and angles of complexes **6**−**8** are summarized in Table 1. Due to the positional disorder noted above, the values reported here correspond to those obtained from the higher-occupancy atoms (full data are provided in the Supporting Information). A clear trend is observed in the metal−nitrogen distances, where Cu−N < Au−N < Ag−N, consistent with the covalent radii of the

https://doi.org/10.1021/acs.inorgchem.6c01837
Inorg. Chem. 2026, 65, 14287−14300

Downloaded from http://pubs.acs.org/inocaj/article-pdf/65/25/14287/6524819/acs.inorgchem.6c01837.pdf by UNIV OF NORTH TEXAS user on 28 July 2026

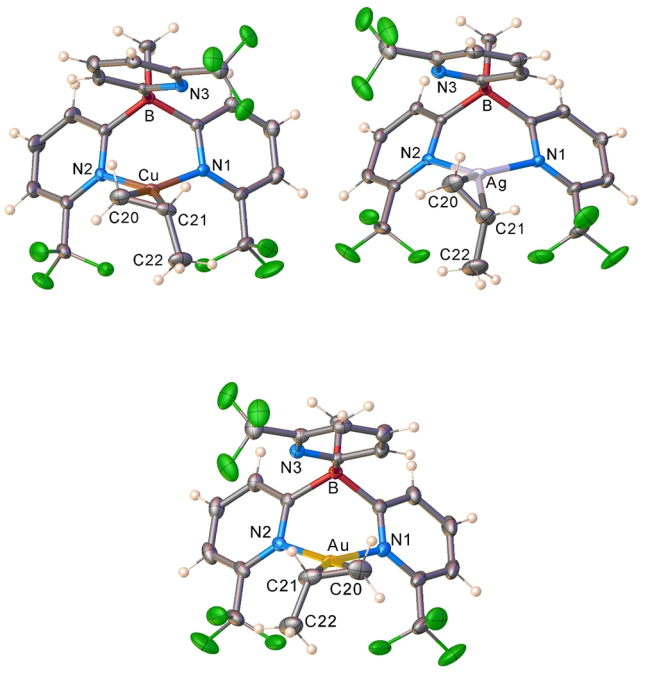


Figure 2. Molecular structures of $[MeB(6\text{-}(CF_3)Py)_3]Cu(C_3H_6)$ (top-left, **6**), $[MeB(6\text{-}(CF_3)Py)_3]Ag(C_3H_6)$ (top-right, **7**), and $[MeB(6\text{-}(CF_3)Py)_3]Au(C_3H_6)$ (bottom, **8**). Thermal ellipsoid plots are shown at a 50% probability level. Only the higher-occupancy orientation of propylene in **6** and **7**, and the higher occupancy gold-propylene unit in **8** is shown for clarity.

Group 11 metals.[55] A similar trend is observed for the M−C distances. Within each complex, the M−CH_2 distance is slightly shorter than the M−$CH(CH_3)$ distance, reflecting perhaps the lesser steric demand at the methylene carbon relative to the methine carbon of the olefin. The C═C bond lengths also vary systematically across the series, with the gold complex having the longest and the silver complex the shortest. For example, the C═C distances in **8** (Au), **6** (Cu), and **7** (Ag) are 1.415(7), 1.373(4), and 1.344(3) Å, respectively. The small lengthening of the C═C bond distance of the silver complex is likely overshadowed by the librational effects and disorder.[46,56] Nevertheless, this trend and these elongations relative to free propylene (1.336(4) Å)[57] reflect varying degrees of π-backbonding, where gold(I) donates the most

Table 1. Selected Bond Distances (Å) and Angles (deg) for Complexes 6−8[a]

parameter	$[MeB(6\text{-}(CF_3)Py)_3]Cu(C_3H_6)$ (**6**)	$[MeB(6\text{-}(CF_3)Py)_3]Ag(C_3H_6)$ (**7**)	$[MeB(6\text{-}(CF_3)Py)_3]Au(C_3H_6)$ (**8**)
C═C	1.373(4)	1.344(3)	1.415(7)
C-CH_3	1.508(3)	1.506(3)	1.509(5)
M-N	2.0087(9)	2.3024(8)	2.169(2)
	2.0118(9)	2.3037(8)	2.266(2)
M-CH_2	2.056(2)	2.3039(16)	2.095(4)
M-CH	2.081(2)	2.4306(16)	2.127(4)
∠NMN	93.41(4)	86.21(3)	83.24(6)
∠CMC	38.77(12)	32.84(6)	39.2(2)
M●●●B	2.9335(12)	3.0950(12)	3.092(2)
Twist angle between NMN and CMC planes	18.1	45.3	10.5

[a]Only values derived from the higher-occupancy atoms of the disordered propylene group were used.

electron density into the π^* orbital of the propylene, resulting in the greatest weakening and lengthening of the C═C bond, followed by copper and silver (see more details in the computational section later). This enhanced π-backbonding is consistent with the strong relativistic stabilization of the 5d orbitals in gold(I), which increases their ability to donate electron density into the olefin π^* orbital. Furthermore, electron-affinity and promotional energy data of Cu(I), Ag(I), and Au(I) indicate that gold is the best σ-acceptor and π-donor in the series.[58,59] These values and trends are similar to those reported for the corresponding C═C bond lengths in the analogous coinage metal ethylene adducts supported by the same ligand for $[MeB(6\text{-}(CF_3)Py)_3]^-$: 1.409(3) Å, 1.360(2) Å, and 1.334(3) Å, respectively.[49] More interestingly, as shown in Figure 2, the propylene coligand in the silver complex **7** adopts a markedly larger twist relative to the N−Ag−N plane (45.30°), compared to its copper analogue **6** (18.10°) and the gold complex **8** (10.51°) (more details given in Figure S1). This substantially greater distortion in **7** is perhaps a sign of weaker interaction between Ag(I) and the propylene group, in particular with a relatively low π-backbonding component. This structural feature is consistent with the trend in metal−olefin bond strengths: Ag−propylene is the weakest interaction, followed by Cu, with Au forming the strongest

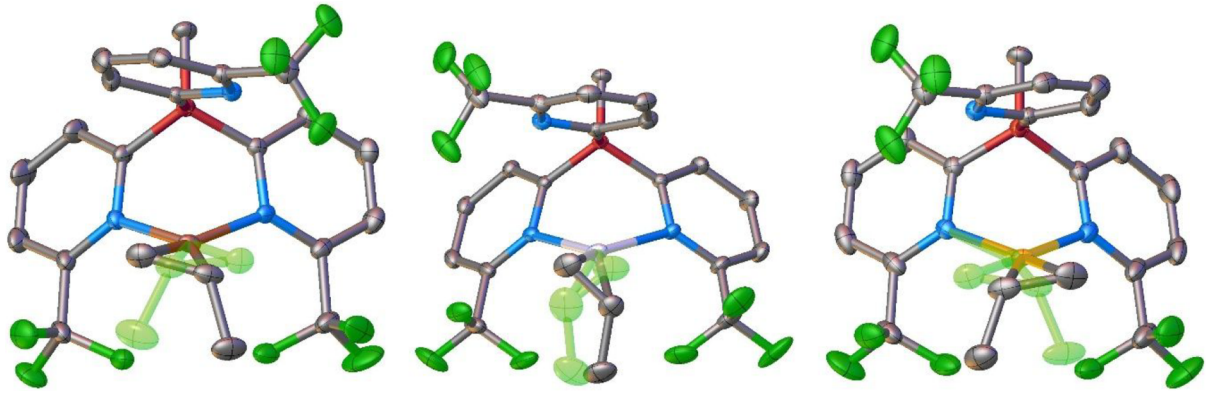


Figure 3. Molecular structures of $[MeB(6\text{-}(CF_3)Py)_3]Cu(C_3H_6)$ (left, **6**), $[MeB(6\text{-}(CF_3)Py)_3]Ag(C_3H_6)$ (middle, **7**), and $[MeB(6\text{-}(CF_3)Py)_3]Au(C_3H_6)$ (right, **8**) showing positional disorder in the propylene groups in **6** and **7** and the Au-propylene moiety in **8**. Hydrogen atoms have been omitted for clarity. Minor component of the disordered moiety in the light-green color.

https://doi.org/10.1021/acs.inorgchem.6c01837
Inorg. Chem. 2026, 65, 14287−14300

Downloaded from http://pubs.acs.org/inocaj/article-pdf/65/25/14287/6524819/acs.inorgchem.6c01837.pdf by UNIV OF NORTH TEXAS user on 28 July 2026

Table 2. Selected ^{1}H and ^{13}C NMR Data in $CDCl_3$ for the Olefinic Protons of the Coordinated Propylene Moiety in Complexes 6−8

	$\delta_H(=CH)$ [$\Delta\delta^c(=CH)$]	$\delta_H(CHH'=)$ [$\Delta\delta^c(CHH'=)$]	$\delta_H(CHH'=)$ [$\Delta\delta^c(CHH'=)$]	$\delta_C(=CH)$ [$\Delta\delta^d(=CH)$]	$\delta_C(CH_2=)$ [$\Delta\delta^d(CH_2=)$]
propylene	5.84	5.00	4.93	136.2	115.9
[MeB(6-$(CF_3)Py)_3$]**Cu**(C_3H_6) (**6**)	4.69[a] [−1.15]	3.91[a] [−1.09]	3.25[a] [−1.68]	100.4[a] [−35.8]	83.5[a] [−32.4]
[MeB(6-$(CF_3)Py)_3$]**Ag**(C_3H_6) (**7**)	5.79[a] [−0.05]	4.72[a] [−0.28]	4.56[a] [−0.37]	116.1[a] [−20.1]	95.2[a] [−20.7]
[MeB(6-$(CF_3)Py)_3$]**Au**(C_3H_6) (**8**)	3.72 [−2.12]	3.00 [−2.00]	2.55 [−2.38]	77.5 [−58.7]	59.1 [−56.8]
	3.91[b] [−1.93][b]	3.20[b] [−1.80][b]	2.49[b] [−2.44][b]	80.8[b] [−55.4][b]	60.2[b] [−55.7][b]

[a]At −40 °C. [b]It belongs to the minor isomer of compound **8** in $CDCl_3$ solution. [c]($\Delta\delta^1H = \delta_{bound} - \delta_{free}$): difference between δ_H of the C*H*, C*H*H′, and CH*H*′ of the free propylene and δ_H of the C*H*, C*H*H′, and CH*H*′ of coordinated propylene, respectively, values shown in [brackets]. [d]($\Delta\delta^{13}C = \delta_{bound} - \delta_{free}$): difference between δ_C of the *C*H and CH_2 of the free propylene and δ_C of the *C*H and CH_2 of coordinated propylene, respectively, values shown in [brackets].

metal−propylene bond. By contrast, the C−CH_3 distances in the propylene coligands remain essentially unchanged across **6**−**8** (at the 3σ limit of standard deviation), indicating that this bond is less affected by the metal−olefin interactions in these molecules. A search in the Cambridge Structural Database (CSD) returned 34 structurally authenticated transition metal η^2-propylene complexes. Of these, as noted earlier, only four copper(I)−propylene complexes[29,42] and one gold(I)−propylene complex (with unresolved propylene disorder),[43] are available for structural comparisons. The C=C bond distance in the copper complex **6** (1.373(4) Å) falls within the expected range of 1.361−1.391 Å found for other Cu−propylene structures.[29,42]

We next investigated the solution behavior of [MeB(6-$(CF_3)Py)_3$]Cu(C_3H_6) (**6**), [MeB(6-$(CF_3)Py)_3$]Ag(C_3H_6) (**7**), and [MeB(6-$(CF_3)Py)_3$]Au(C_3H_6) (**8**) by NMR spectroscopy. Based on the solid-state single crystal structures, the unbound pyridyl arm is oriented above the propylene moiety, introducing ring current effects that influence the ^{1}H NMR spectra of these complexes. The ^{19}F NMR of **6**−**8** each displayed a single resonance at room temperature, indicating rapid exchange between the N-coordinated and noncoordinated pyridyl arms on the NMR time scale. The ^{1}H NMR spectra of **6** and **7** were recorded at −40 °C in $CDCl_3$ solution to slow the fast exchange of propylene (for **6**, a slight excess of propylene gas was added), which allowed sharp resonances for the coordinated propylene ligands to be observed. The ^{1}H NMR data (Table 2) showed upfield chemical shifts for the olefinic proton signals compared to those of free propylene in all the complexes. For the copper complex **6**, the β-olefinic proton (=C*H*) is shifted upfield by 1.15 ppm, while the α-olefinic protons (C*HH*′=) exhibited shifts of 1.09 and 1.68 ppm relative to free propylene. The large upfield shifts are partly attributable to the ring current effect of the flanking pyridyl moieties. For comparison, the β- and α-olefinic protons in [$H_2B(3,5\text{-}(CF_3)_2Pz)_2$]Cu($C_3H_6$) (**1**), which lacks such a ring current influence, show much smaller shifts of approximately 0.33 and 0.20 ppm, respectively. The silver complex **7** displayed the smallest upfield chemical shifts, whereas the gold complex **8** showed the largest shifts of the α- and β-olefinic proton. Interestingly, the ^{1}H NMR spectrum of complex **8** revealed two isomeric species in a 77:23 ratio. However, this behavior is not exclusive to this system. The presence of two isomers arising from different orientations of the propylene methyl group relative to the ligand framework (Figure S2) has precedent in a few d-block complexes, such as [{[$HB(3,5\text{-}(Me)_2Pz)_3$]H}Pt($C_3H_6$)($CH_3$)][$BAr^F{}_4$][50] and a gold-propylene complex.[43]

The ^{13}C NMR shift is a valuable parameter for characterizing the metal−propylene bonds in these complexes,[60−62] as the high-field coordination shift of the olefin carbons increases with the π-back-donation, and it is less influenced by ring current effects compared to the ^{1}H NMR shift. In complexes **6**−**8**, the olefinic β-(=CH) and α-(CH_2=) carbons of the coordinated propylene exhibit upfield shifts relative to free propylene (Table 2). For example, in the copper complex **6**, these carbons resonated at δ 100.4 and 83.5 ppm, respectively, whereas in the major isomer of the gold complex **8**, they appeared at δ 77.5 and 59.1 ppm. Overall, gold complexes showed the largest upfield shift, while the silver complexes displayed the smallest shift. This trend mirrors the observation in ^{1}H NMR shift and can be attributed to the σ-acceptor and π-back bonding interactions between the coinage metal ions and propylene. These observations in NMR studies were consistent with findings noted above for solid-state structure regarding the interaction strength of coinage metal ions with olefins, as well as observations of the stability of propylene complexes under reduced pressure.

Raman spectroscopy is a powerful tool for probing shifts in the C=C stretching frequency upon metal ion coordination, providing insights into the strength of metal−olefin bonding interaction. It should be noted, however, that these molecules have pyridyl moieties that could also produce C=C and C=N stretching bands in the same region, interfering with the unambiguous assignment of the propylene C=C stretch. Nevertheless, peak assignment could be made, at least tentatively, based on a spectra comparison between the propylene complexes and the propylene-free copper adduct (see below and Figure S6). A clear reduction in the C=C stretching frequency was observed for the coordinated propylene in copper complex **6** (1546 cm^{-1}) and gold complex **8** (1493 cm^{-1}) relative to free propylene (1648 cm^{-1}). In the case of the silver complex **7**, fluorescence hindered the acquisition of high-quality Raman data, preventing reliable assignment of the C=C stretching vibration (1575 cm^{-1}, Figure S10). In the IR spectrum, however, a band at 1586 cm^{-1} could be tentatively assigned to the C=C stretch of the coordinated propylene ligand (Figure S11), again based on a comparison of the spectra data of complex **7** to that of the propylene-free silver species. As expected, the gold complex **8** exhibited the lower C=C stretching frequency than the copper analog **6** and the silver analog **7**, consistent with stronger alkene→metal σ-donation and metal→alkene π-backbonding in the gold(I) complex.

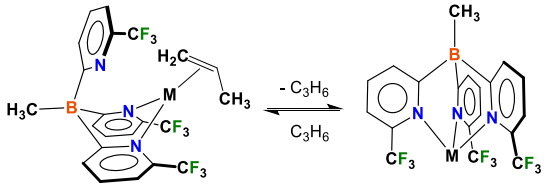
When complexes [MeB(6-$(CF_3)Py)_3$]Cu(C_3H_6) (**6**) and [MeB(6-$(CF_3)Py)_3$]Ag(C_3H_6) (**7**) were placed under reduced

https://doi.org/10.1021/acs.inorgchem.6c01837
Inorg. Chem. 2026, 65, 14287−14300

Downloaded from http://pubs.acs.org/inocaj/article-pdf/65/25/14287/6524819/acs.inorgchem.6c01837.pdf by UNIV OF NORTH TEXAS user on 28 July 2026

pressure, the coordinated propylene was cleanly removed (Scheme 2), affording the corresponding white solids, which

Scheme 2. Reversible Propylene Desorption and Absorption Chemistry of Complexes 6 and 7 and into 9 and 10



M = Cu (6); Ag (7) M = Cu (9); Ag (10)

exhibit poor solubility in weakly coordinating solvents such as dichloromethane, chloroform, and hexanes, but dissolve readily in more polar media such as DMSO or acetonitrile. Crystallization from tetrahydrofuran furnished high-quality single crystals, enabling unambiguous structural determination of the propylene-free species, [MeB(6-(CF$_3$)Py)$_3$]Cu (**9**) and [MeB(6-(CF$_3$)Py)$_3$]Ag (**10**), as illustrated in Figure 4. Complexes **9** and **10** feature the κ^3-*N,N,N*-bound coordination of tris(pyridyl)borate. The bond lengths trend (Cu−N < Ag−N) and the angle trend (N−Cu−N > N−Ag−N) observed in **9** and **10** follow the expected covalent radii of the metals, with copper smaller than silver.[55] For the copper system, the Cu●●●B distance contracts upon loss of propylene (2.7805(18) Å in **9** vs. 2.9335(12) Å in **6**), while the silver analogue shows the opposite trend, with an elongated Ag●●●B separation in **10** compared to **7** (3.254(2) vs. 3.0950(12) Å).

The packing diagram of **9** shows that it crystallizes with one of the CF$_3$ groups of the adjacent molecule covering the open space of the copper site (Figure 5), but the closest intermolecular Cu●●●F separations are at 4.070(3) Å, which are longer than the sum of the van der Waals contact distances of Cu and F (3.84 Å). There are close intramolecular Cu●●●F separations within this limit, with the closest at 2.821(2) Å. Thus, [MeB(6-(CF$_3$)Py)$_3$]Cu exists as a monomeric species in the solid state. Packing diagrams of **10** show that the open coordination site of the silver atom in [MeB(6-(CF$_3$)Py)$_3$]Ag faces the H$_3$C−B moiety of the adjacent molecule, with a closest intermolecular Ag●●●H separation of 2.8962(3) Å. This separation is longer than the sum of covalent radii of silver and hydrogen (1.77 Å)[55] but within the van der Waals contact of the two atoms (3.73 Å).[63] Overall, these long-range interactions are perhaps the reason for the crystallization of [MeB(6-(CF$_3$)Py)$_3$]Ag (Figure 5) in forming linear chains.

The isolation of copper and silver complexes in the absence of supporting coligands (e.g., without the propylene co-ligand in **6** and **7**) is possible, as seen in the more extensively studied poly(pyrazolyl)borate ligand-supported systems, but when isolable, such systems mostly adopt a dinuclear species,[64−73] or in a rare case, a trinuclear species,[74] or an infinite chain[75,76] formulations. Compounds **9** and **10** represent very rare, three-coordinate, trigonal pyramidal d-block metal complexes, similar to that reported recently involving a tris(pyrazolyl)-borate, {[HB(3-^{t}Bu-5-^{i}Pr-Pz)$_3$]Co}[BAr$^F_4$].[77] Such a coordination geometry is more common in main-group chemistry, for example, [MeB(6-(CF$_3$)Py)$_3$]Tl.[78] Trigonal pyramidal coordination, however, has been observed in four-coordinate d-block complexes.[79−82] Attempts to isolate the propylene-free gold analogue by reacting the potassium ligand precursor with AuCl in the absence of a supporting coligand, such as propylene, resulted in the formation of a black precipitate, indicating decomposition of the gold precursor. HR-MS analysis of the decomposition mixture revealed the presence of the protonated ligand [MeB(6-(CF$_3$)Py)$_3$]H. Similarly, prolonged exposure of the isolated solid **8** to reduced pressure under heating also led to decomposition.

Furthermore, theoretical calculations were performed to assess the bonding and electronic properties of the propylene complexes reported here. Different orientations of the propylene unit relative to the [MeB(6-(CF$_3$)Py)$_3$]M core were examined (Figure S27), showing only slight energy differences (<0.5 kcal/mol) (Table S6), which indicates the feasibility of multiple arrangements for the metal−propylene coordination. This also explains the observed positional disorder in the crystal structures. The calculated geometrical parameters for the crystallized species are in line with experimental values (Table S7). A notable difference is observed between the calculated and experimental twist angles of silver complex **7** (21.41° vs 45.30°, respectively), which is presumably caused by crystal packing effects that are not taken into account in the molecular model. In addition, the small difference in energy between the several orientations of the coordinated propylene ligand (Table S6) suggests an easy rotation.

The isolable, propylene free [MeB(6-(CF$_3$)Py)$_3$]Cu (**9**) and [MeB(6-(CF$_3$)Py)$_3$]Ag (**10**) species and the calculated [MeB(6-(CF$_3$)Py)$_3$]Au counterpart exhibit a charge distribu-

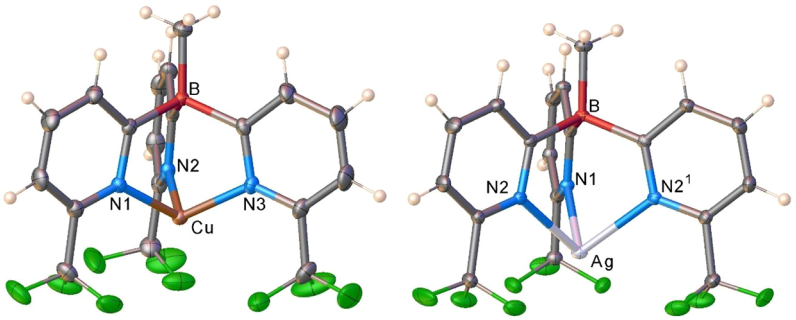


Figure 4. Molecular structures of monomeric species [MeB(6-(CF$_3$)Py)$_3$]Cu (left, **9**) and [MeB(6-(CF$_3$)Py)$_3$]Ag (right, **10**). Thermal ellipsoid plots are shown at a 50% probability level. Selected bond distances (Å) and angles (°) for **9**: Cu−N, 1.9826(14), 1.9814(14), 1.9789(14); N−Cu−N, 99.75(6), 103.33(6), 103.30(6); B●●●Cu, 2.7805(18), and for **10**: Ag−N, 2.3248(17), 2.3305(12), 2.3304(12); N−Ag−N, 87.74(4), 87.74(4), 87.69(6); B●●●Ag, 3.254(2).

https://doi.org/10.1021/acs.inorgchem.6c01837
Inorg. Chem. 2026, 65, 14287−14300

Downloaded from http://pubs.acs.org/inocaj/article-pdf/65/25/14287/6524819/acs.inorgchem.6c01837.pdf by UNIV OF NORTH TEXAS user on 28 July 2026

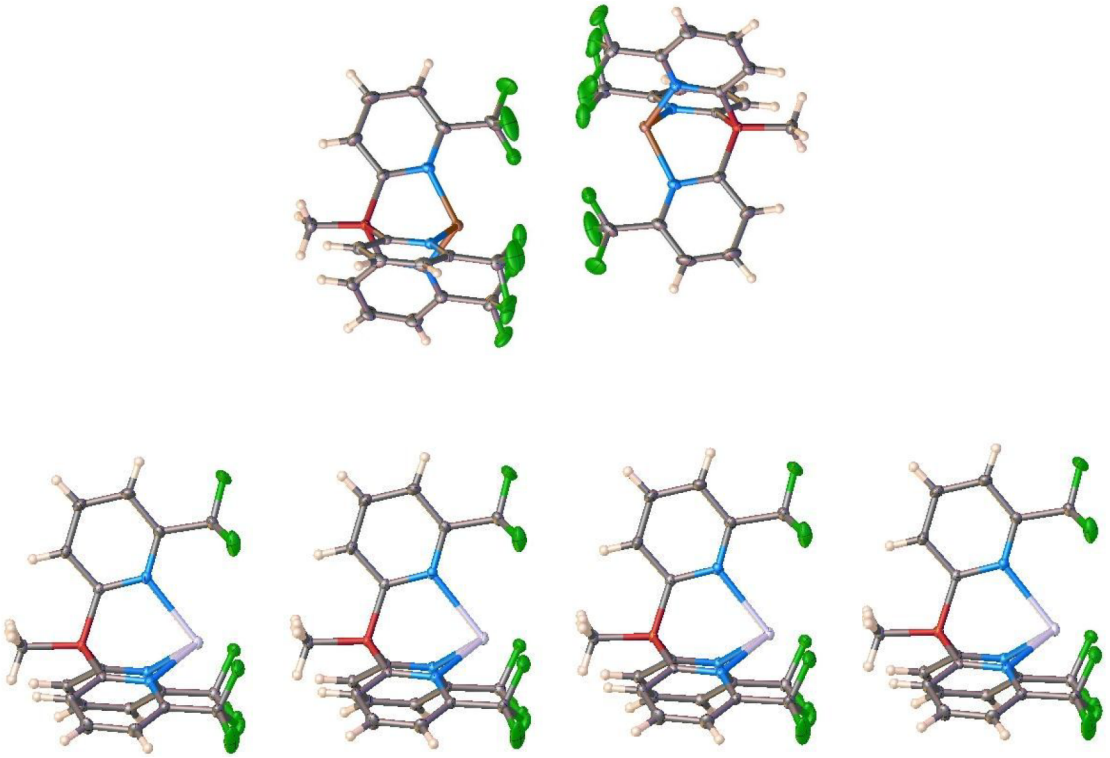


Figure 5. Part of the packing diagram of [MeB(6-(CF_3)Py)$_3$]Cu (top, **9**) and [MeB(6-(CF_3)Py)$_3$]Ag (bottom, **10**) illustrating the arrangement of neighboring molecules.

tion on the coinage metal center of 0.27, 0.30, and 0.23 lel respectively, owing to a net [MeB(6-(CF_3)Py)$_3$]→M charge transfer, which is larger for Au, followed by Cu and Ag. This indicates a substantial stabilization from interaction energy upon tris(pyridyl)borate ligand coordination. The resulting positively charged metal center indicates the presence of a localized electron-deficient region at the metal site, and the molecular electrostatic potential (MEP) over the van der Waals surface helps identify and quantify the electron-deficient (acidic) sites within the complex (Figure S28).[83] These features have been rationalized as σ-holes,[83−85] accounting for Lewis acidic regions, displaying a maxima in the electrostatic potential ($V_{S,max}$) over the van der Waals surface. For **9**, **10,** and the gold counterpart, the MEP potential surface shows a positive region on metal complexes with values of $V_{S,max}$ over the Cu, Ag, and Au sites of 5.8, 18.4, and 2.3 kcal/mol, respectively. This suggests that the σ-hole is stronger in the silver compound, which explains the preference for linearly ordered extended structures in the solid-state structure of **10** (Figure 5) compared to **9**.

The calculated interaction energy between [MeB(6-(CF_3)-Py)$_3$]$^-$ and M$^+$ amounts to −224.2 kcal/mol for the Cu species **9**, decreasing to −180.4 kcal/mol for the Ag complex **10** and to −208.7 kcal/mol for the gold counterpart (Table S8). The electrostatic character dominates these interactions. Interestingly, upon propylene coordination to the metal site, the [MeB(6-(CF_3)Py)$_3$]$^-$ and M(C_3H_6)$^+$ interaction energy decreases to an average of −169.6, −146.5, and −165.5 kcal/mol, respectively, revealing that the bonding characteristics of the coinage metal center are shared between both the tris(pyridyl)borate and propylene ligands. The resulting charge at the metal amounts to 0.32, 0.35, and 0.34 lel, which is more positive in comparison to the [MeB(6-(CF_3)Py)$_3$]M parent. This indicates greater electron loss from the metal upon coordination to propylene. The related interaction energy between the [MeB(6-(CF_3)Py)$_3$]M and (C_3H_6) fragments is calculated to −42.8 kcal/mol (average considering different orientations of propylene) for [MeB(6-(CF_3)Py)$_3$]Cu(C_3H_6) (**6**), decreasing to −27.9 kcal/mol in [MeB(6-(CF_3)Py)$_3$]Ag-(C_3H_6) (**7**), and increasing to −63.6 kcal/mol for [MeB(6-(CF_3)Py)$_3$]Au(C_3H_6) (**8**), pointing to Au > Cu > Ag order of stabilization within the series (Table S9). The calculated thermodynamic parameters consequently exhibit a Gibbs free energy change of −35.8 kcal/mol for the [MeB(6-(CF_3)Py)$_3$]Au + C_3H_6 → [MeB(6-(CF_3)Py)$_3$]Au(C_3H_6) (**8**) reaction, driven by a favorable enthalpy change (Table S10), which is lower at −10.7 and −7.3 kcal/mol for the silver (**7**) and copper (**6**) counterparts at −40 °C. These values are −35.3, −10.0, and −6.5 kcal/mol at −20 °C, consistent with the more labile behavior of the lighter counterparts relative to the gold species.

The bonding scheme involving the propylene coordination to the respective metal center, that is, [MeB(6-(CF_3)Py)$_3$]M and C_3H_6 interaction, is comprised of π-backdonation and σ-donation, ascribed to the M → π_2*-C_3H_6 and M ← π_1-C_3H_6 contributions (Figure 6). The metal→propylene π-back donation is relatively stronger compared to the propylene→ metal σ-donation in all these metal complexes. This trend is similar to that found in the [Ph_2B(3-(CF_3)Pz)$_2$]Cu(C_2H_4) species.[86] Specifically, corresponding energy for each of such bonding elements amounts to −28.3 and −17.6 kcal/mol for [MeB(6-(CF_3)Py)$_3$]Cu(C_3H_6) (**6**), decreasing to −14.9 and −12.9 kcal/mol, respectively, in [MeB(6-(CF_3)Py)$_3$]Ag(C_3H_6) (**7**), in agreement with decreased interaction energy. For the gold counterpart **8**, the corresponding bonding interactions are enhanced as evident from −46.6 and −36.5 kcal/mol, respectively, indicating an overall preference for Au > Cu >

https://doi.org/10.1021/acs.inorgchem.6c01837
Inorg. Chem. 2026, 65, 14287−14300

Downloaded from http://pubs.acs.org/inocaj/article-pdf/65/25/14287/6524819/acs.inorgchem.6c01837.pdf by UNIV OF NORTH TEXAS user on 28 July 2026

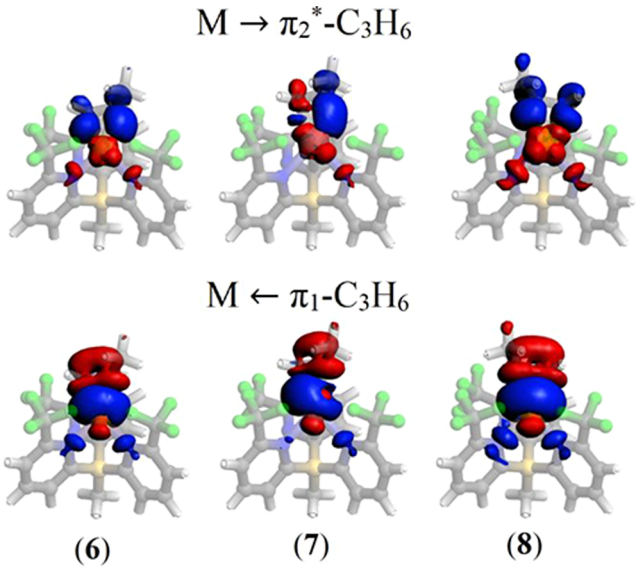


Figure 6. Individual contributions to the orbital interaction, from the Natural Orbitals for Chemical Valence extension of the EDA method (EDA-NOCV), are given for $[MeB(6\text{-}(CF_3)Py)_3]Cu(C_3H_6)$ (**6**), $[MeB(6\text{-}(CF_3)Py)_3]Ag(C_3H_6)$ (**7**), and $[MeB(6\text{-}(CF_3)Py)_3]Au(C_3H_6)$ (**8**). Charge transfer from red to blue.

Ag stabilization. Such values are similar to the related ethylene counterparts ($[MeB(6\text{-}(CF_3)Py)_3]M(C_2H_4)$,[49] which exhibit −29.4/−17.6 kcal/mol in $[MeB(6\text{-}(CF_3)Py)_3]Cu(C_2H_4)$ for M → π_2*-C_2H_4 and M ← π_1-C_2H_4 backbonding and σ-donor elements, respectively, varying to −20.3/−14.1 kcal/mol for silver and to −48.8/−36.1 kcal/mol for the gold counterpart, where a difference in the Ag → π_2*-C_2H_4 could be a result of the shorter Ag−C bond in the ethylene ligand (or a relatively shorter Ag−C in the ethylene counterpart is a reflection of the stronger Ag-ethylene bonding). The computed values for the $[MeB(6\text{-}(CF_3)Py)_3]M(C_3H_6)$ species in turn lead to a variable population of both π_1-C_3H_6 and π_2*-C_3H_6 orbitals of 1.93/0.17 lel in **6**, 1.91/0.09 lel in **7**, and of 1.71/0.34 lel in **8** (vs 2.0 and 0.0 lel in free propylene), further supporting the more significant σ-π-interaction in the heaviest member, leading to a more stabilized propylene coordination in comparison to copper and silver. Lastly, the calculated[13] ^{13}C- and ^{1}H NMR parameters of **6**−**8** show good agreement with the experimental data (Table S11), supporting the evaluated bonding scheme and the related quantification of the interaction energy features.

A comparison of computed interaction energy values of propylene and ethylene coordination to the M center shows that $[MeB(6\text{-}(CF_3)Py)_3]M$ and C_3H_6 have average values of −29.0, −14.1, and −45.9 kcal/mol for Cu, Ag, and Au species, respectively, while for $[MeB(6\text{-}(CF_3)Py)_3]M$ and C_2H_4, they are −44.7, −30.0, and −63.3 kcal/mol for the respective interaction.[49] This suggests a more stable coordination for the ethylene counterparts (C_2H_4) and thus a more labile situation in the propylene (C_3H_6) coordination. Structurally, the propylene ligand (CMC plane) exhibits a twisted arrangement relative to the NMN plane (Table 1), with angles of 18.10, 45.30, and 10.51° for Cu, Ag, and Au species, respectively. These can be contrasted with the twist angles of 5.17, 4.11, and 2.47° observed in the ethylene counterparts, indicating a more distorted coordination environment for the propylene complexes. This likely results from unfavorable steric

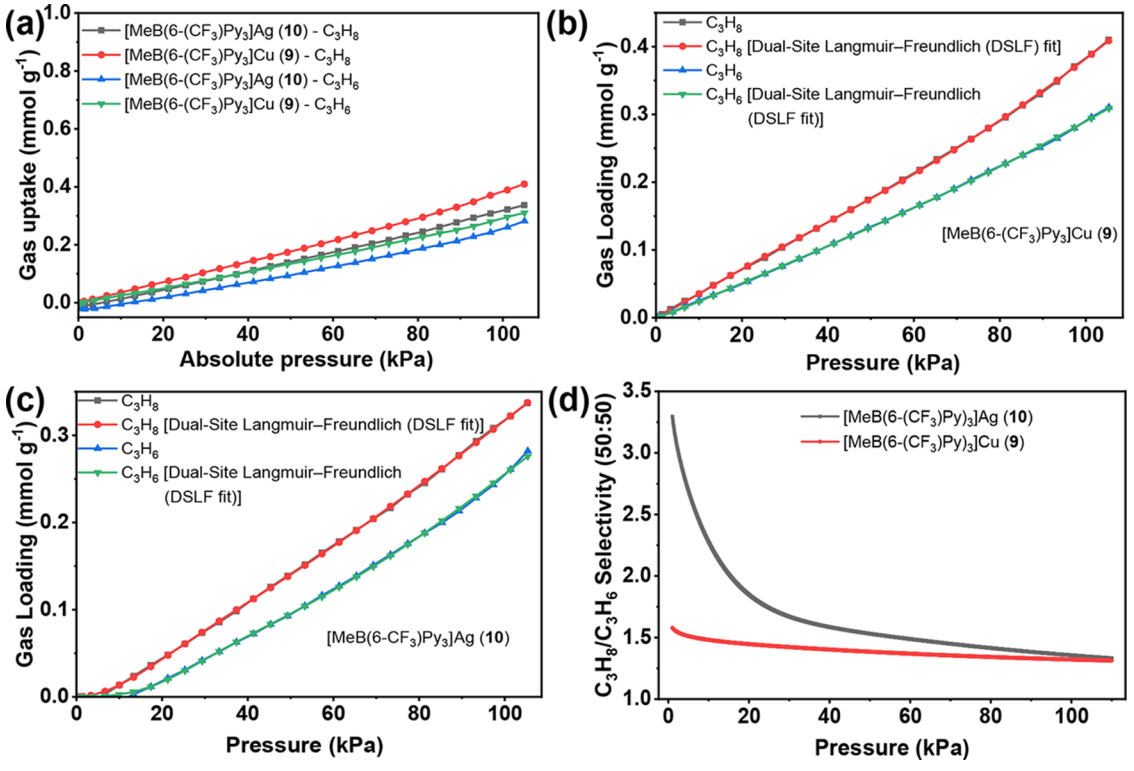


Figure 7. (a) Single-component adsorption isotherms of C_3H_8 and C_3H_6 for $[MeB(6\text{-}(CF_3)Py)_3]Cu$ (**9**) and $[MeB(6\text{-}(CF_3)Py)_3]Ag$ (**10**) at 298 K and pressures up to 1 bar. (b, c) Dual-Site Langmuir−Freundlich (DSLF) fits of the adsorption data. (d) IAST selectivity for C_3H_8/C_3H_6 separation at 298 K for **9** and **10**.

https://doi.org/10.1021/acs.inorgchem.6c01837
Inorg. Chem. 2026, 65, 14287−14300

Downloaded from http://pubs.acs.org/inocaj/article-pdf/65/25/14287/6524819/acs.inorgchem.6c01837.pdf by UNIV OF NORTH TEXAS user on 28 July 2026

interactions between the tris(pyridyl)borate and the methyl group of the propylene.

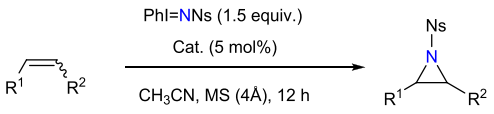
Considering the reversible interaction of [MeB(6-(CF_3)-Py)$_3$]Cu (**9**) and [MeB(6-(CF_3)Py)$_3$]Ag (**10**) with propylene observed in solution studies, we further examined their solid-state behavior as potential adsorptive materials. It is worth noting that [H_2B(3,5-(CF_3)$_2$Pz)$_2$]Cu(C_3H_6) (**1**)[29] involving a fluorinated bis(pyrazolyl)borate is an interesting nonporous material that displays outstanding propylene-propane separation capabilities. In this work, fluorinated materials **9** and **10** were evaluated as candidates for the selective separation of propane/propylene (C_3H_8/C_3H_6) mixtures. Single-component adsorption isotherms measured at 298 K and 1 bar reveal a clear preferential affinity for C_3H_8 over C_3H_6 (Figure 7a). The copper compound **9** and the silver analog **10** exhibit maximum C_3H_8 uptake capacities of 0.41 and 0.33 mmol g^{-1}, respectively, exceeding their corresponding C_3H_6 uptakes of 0.31 and 0.28 mmol g^{-1}. These values correspond to C_3H_8/C_3H_6 adsorption ratios of 1.36 for **9** and 1.16 for **10** at 298 K. The preferential adsorption of C_3H_8 over C_3H_6 is notable, as it contrasts with the behavior of coinage-metal materials including the bis(pyrazolyl)borate species {[H_2B(3,5-(CF_3)$_2$Pz)$_2$]Cu}$_3$ derived from [H_2B(3,5-(CF_3)$_2$Pz)$_2$]Cu-(C_3H_6) (**1**). The solid samples of {[H_2B(3,5-(CF_3)$_2$Pz)$_2$]Cu}$_3$ favor propylene binding through π-complexation with impressive selectivity, regenerating **1**.[29] It also preferentially binds ethylene over ethane.[74] In the present system, however, the fluorinated poly(pyridyl)borate framework likely dominates the guest recognition process, promoting stronger interactions with paraffinic molecules.

Because industrial separations often require high selectivity at low partial pressures, particularly for trace component removal, the separation performance was further evaluated using Ideal Adsorbed Solution Theory (IAST). The calculated IAST selectivity for an equimolar (50:50) mixture of C_3H_8/C_3H_6 at 298 K and 1 kPa is 1.58 for **9** and 3.2 for **10** (Figure 7b–d), confirming the preferential adsorption of propane in the silver-based material at low pressure. The highly polarizable C–H bonds of propane can adopt favorable orientations that enable multiple weak interactions with the fluorinated environment, including C–H···F and C–H···π contacts, whereas the more rigid propylene molecule is less able to maximize such interactions.[87−89] These results suggest that adsorption in **9** and **10** in a solid state is controlled primarily by framework–guest interactions rather than direct metal–olefin coordination.

Complexes supported by poly(pyridyl)borate ligands remain comparatively underexplored,[90] and their applications in catalysis are even less reported. Recently, our group demonstrated that silver and rhodium complexes bearing poly(pyridyl)borate frameworks are effective catalysts for alkene C–H activation[91] and for C–C silylation of cyclopropyl acetates,[92] respectively. Beyond these examples, a few other groups have investigated related systems, including platinum- and zinc-based catalysts for oxidation reactions,[93−96] vanadium- and magnesium-supported complexes for olefin polymerization,[97−99] and ruthenium derivatives for the dehydrogenation of ammonia borane.[100] In this work, we extend this chemistry by employing coinage-metal complexes within this ligand platform for nitrene transfer in aziridination reactions. Aziridines are valuable synthetic intermediates due to their utility in accessing a wide range of functional molecules.[101] While both metal-free[102−104] and metal-mediated[105−107] approaches to aziridination have been reported, transition-metal catalysis has attracted particular attention because of its potential to control reactivity and selectivity.[101] As noted by Pérez and co-workers, an effective aziridination catalyst should display high activity toward terminal and less reactive olefins (e.g., 1-hexene) and operate without requiring an excess of olefin substrate.[108]

Guided by these criteria, aziridination reactions in this study were conducted using a variety of terminal and internal alkenes (1.0 equiv), with PhI=NNs (1.5 equiv) employed as the nitrene source. Under the reaction conditions, the copper complex [MeB(6-(CF_3)Py)$_3$]Cu (**9**) proved to be an effective catalyst, affording aziridination products in good yields (Table 3). Notably, even nonactivated terminal alkenes such as 1-hexene and 3,3-dimethyl-1-butene, which are typically challenging for this transformation, underwent aziridination in moderate yields. These results are comparable to those of reactions catalyzed by poly(pyrazolyl)borate copper catalysts such as [HB(3,5-(CF_3)$_2$Pz)$_3$]Cu(C_2H_4)[109] or [HB(3,4,5-(Br)$_3$Pz)$_3$]Cu(MeCN).[108] Importantly, no excess olefin was required, indicating that the copper catalyst **9** satisfies the key performance benchmarks for improved aziridination catalysts. Additionally, catalyst **9** is also capable of promoting the reaction with propylene when used in excess, affording the corresponding aziridine adduct in a good yield. Upon addition of PhI=NNs to a solution of **9**, an immediate color change to green was observed, consistent with the formation of a higher oxidation-state copper species, likely a Cu(II) species, as an intermediate. Such behavior is commonly reported in copper-catalyzed nitrene-transfer processes.[105] In contrast, the silver complex [MeB(6-(CF_3)Py)$_3$]Ag (**10**) and the gold complex [MeB(6-(CF_3)Py)$_3$]Au(C_3H_6) (**8**) exhibited markedly diminished catalytic activity (see more details in Table S12). Among the substrates examined, only styrene showed some conversions, and even then the yields were low. There was a formation of black precipitates when gold catalyst **8** was employed, indicating catalyst decomposition under the reaction conditions. In contrast, no visible decomposition was detected with silver catalyst **10**; however, its low catalytic efficiency is likely due to the slower nitrene transfer.

Table 3. Reaction Yields (%) for Nitrene Transfer Reactions Using Complex [MeB(6-(CF_3)Py)$_3$]Cu (9) as Catalyst



entry	alkene	% yields
1	styrene	>98
2	cyclohexene	70
3	*t*-stilbene	>98
4	1-hexene	70
5	3,3-dimethyl-1-butene	64
6	propylene[a]	92

[a]Used in excess.

CONCLUSION

Successful isolation and detailed studies, including structural data of a series of coinage metal-propylene complexes supported by a tris(pyridyl)borate, are reported. Among the coinage metals, gold(I) affects the propylene moiety most

https://doi.org/10.1021/acs.inorgchem.6c01837
Inorg. Chem. 2026, 65, 14287−14300

Downloaded from http://pubs.acs.org/inocaj/article-pdf/65/25/14287/6524819/acs.inorgchem.6c01837.pdf by UNIV OF NORTH TEXAS user on 28 July 2026

strongly, as reflected by the large upfield shifts of the olefinic carbon signals in the NMR spectra and the increased C=C bond length. The copper(I) and silver(I) complexes display reversible propylene binding, and desorption of the olefin affords propylene-free species with rare trigonal pyramidal coordination geometries, which represent the only such examples of poly(pyridyl)borate ligands with d-block elements. Theoretical investigations provided useful information on the bonding and electronic structure of coinage metal propylene and propylene-free complexes supported by tris(pyridyl)borate ligands. Minimal energy differences between multiple propylene orientations indicate structural flexibility of the propylene moiety, consistent with experimentally observed disorder. Charge distribution and molecular electrostatic potential analyses reveal positively polarized metal centers with σ-hole character, most pronounced for silver, rationalizing its distinct solid-state organization in the trigonal pyramid **10**. Interaction energy calculations show strong ligand-to-metal electrostatic stabilization, which decreases upon propylene coordination as bonding is shared between ligands. Comparative thermodynamic and interaction data establish a stability trend of Au > Cu > Ag for propylene binding, with gold complexes exhibiting the most favorable energetics. Orbital analysis indicates that bonding is dominated by metal-to-propylene π-backdonation complemented by σ-donation from propylene to the metal ion, with the strongest synergistic interaction observed for gold, leading to enhanced stabilization of the coordinated propylene relative to copper and silver analogs. Adsorption studies of the desorbed materials reveal a higher affinity for propane over propylene, indicating that host–guest interactions within the fluorinated ligand environment dominate rather than direct metal–olefin coordination. The copper material also shows greater selectivity than the silver analog at low pressure. Preliminary catalytic studies demonstrate that the copper complex is active toward olefin aziridination, including both terminal and less-reactive alkenes, without requiring excess substrate (except in the case of gaseous propylene). These results highlight the versatility of fluorinated poly(pyridyl)borate-supported coinage-metal complexes for studying metal–olefin bonding, adsorption behavior, and metal-mediated processes.

EXPERIMENTAL SECTION

General Information

All preparations and manipulations were carried out under an atmosphere of purified nitrogen using standard Schlenk techniques or in a vacuum atmosphere single-station drybox equipped with a −25 °C refrigerator. Dichloromethane, acetonitrile, and hexane were dried by passing HPLC-grade solvent through a solvent purification system (SPS, Innovative Technologies Inc.) and stored in Straus flasks. NMR spectra were recorded at 25 °C on a JEOL Eclipse 400 spectrometer (^{1}H, 400 MHz; ^{13}C, 101 MHz, ^{19}F, 376 MHz), or a JEOL Eclipse 500 (^{1}H, 500 MHz; ^{13}C, 126 MHz; and ^{19}F, 471 MHz), unless noted. All the spectral data were processed on MNova. ^{1}H and ^{13}C NMR spectra are referenced to the solvent peak (^{1}H, $CDCl_3$ δ 7.26, $(CD_3)_2SO$ δ 2.50; ^{13}C, $CDCl_3$ δ 77.16, $(CD_3)_2SO$ δ 39.52). ^{19}F NMR values were referenced to external $CFCl_3$. ^{1}H, ^{13}C, and ^{19}F NMR chemical shifts are reported in ppm and coupling constants (J) are reported in Hertz (Hz). Raman data were collected on a Thermo Fisher Scientific DXR Raman microscope, or JASCO NRS-5500 spectrometer with a HeNe laser source of 633 nm, by placing pure solid materials on a glass slide. The IR data were collected on a JASCO FT/IR-4X spectrometer with an ATR attachment and at a resolution of 2.0 cm^{-1}. Abbreviations used for signal assignments: Py = pyridyl, Me = Methyl, s = singlet, d = doublet, t = triplet, q = quartet, m = multiplet, br = broad peak, brs = broad singlet, free C_3H_6 = free propylene, Prop = bound propylene moiety, Py^m and Prop^m and B-CH_3^m belong to the minor isomer of compound **8**. $[MeB(6\text{-}(CF_3)Py)_3]K$,[49] $AuCl(SMe_2)$,[110] and PhI=NNs[111] were synthesized as previously reported. All other reactants and reagents were purchased from commercial sources. NMR solvents were purchased from Cambridge Isotopes Laboratories and used as received.

Synthetic Procedures

Safety: *No uncommon hazards were noted during this study.*

$[MeB(6\text{-}(CF_3)Py)_3]Cu(C_3H_6)$ (6). To a mixture of $[MeB(6\text{-}(CF_3)Py)_3]K$ (100 mg, 0.199 mmol, 1 equiv) and $[CuOTf]_2$•PhMe (52 mg, 0.100 mmol, 0.5 equiv) in a 50 mL Schlenk flask, anhydrous dichloromethane (20 mL) was added, and then propylene (1 atm) was bubbled into the solution. The reaction mixture was stirred for 3 h and then cannula-filtered through a Celite-packed frit to remove KOTf. The solution was concentrated under reduced pressure, and the compound was recrystallized from dichloromethane saturated with propylene and layered with hexane, then kept at −20 °C to obtain colorless X-ray quality single crystals of $[MeB(6\text{-}(CF_3)Py)_3]Cu(C_3H_6)$. Yield: 97 mg (86%). ^{1}H NMR (400 MHz, $CDCl_3$, −40 °C): δ (ppm) 7.75–7.62 (m, 6H, Py), 7.43 (t, J = 7.6 Hz, 3H, Py), 4.69 (m, 1H, C*H*, Prop), 3.91 (m, 1H, C*H*H′, Prop), 3.25 (d, J = 10.9 Hz, 1H, CH*H*′, Prop), 0.69 (br, 3H, CH_3, Prop), 0.49 (s, 3H, B–CH_3). ^{13}C{^{1}H} NMR (101 MHz, $CDCl_3$, −40 °C): δ (ppm) 186.6 (q, $^1J_{C-B}$ = 56.5 Hz, B-Py), 145.5 (q, $^2J_{C-F}$ = 33.0 Hz, *C*-CF_3), 135.4 (s, Py), 132.2 (s, Py), 122.0 (q, $^1J_{C-F}$ = 274.4 Hz, CF_3, Py), 115.7 (s, Py), 100.4 (s, Prop), 83.5 (s, Prop), 18.8 (s, Prop), 12.7 (q, $^1J_{C-B}$ = 34.4 Hz, B-CH_3). ^{19}F NMR (376 MHz, $CDCl_3$, −40 °C): δ (ppm) −66.12 (s). HR-MS [ESI, positive ion mode ESI-TOF]: m/z for $C_{19}H_{12}B_1F_9N_3Cu_1$ $[M - C_3H_6 + H]^+$ calcd 528.0355, found 528.0381.

$[MeB(6\text{-}(CF_3)Py)_3]Ag(C_3H_6)$ (7). To a mixture of $[MeB(6\text{-}(CF_3)Py)_3]K$ (100 mg, 0.198 mmol, 1 equiv) and AgOTf (51 mg, 0.198 mmol, 1 equiv) in a 50 mL Schlenk flask covered with aluminum foil, anhydrous dichloromethane (20 mL) was added, and then propylene (1 atm) was bubbled into the solution. The reaction mixture was stirred for 3 h and then cannula-filtered through a Celite-packed frit to remove KOTf. The solution was concentrated under reduced pressure, and the compound was recrystallized from dichloromethane saturated with propylene and layered with hexane and kept at −20 °C to obtain colorless X-ray quality single crystals of $[MeB(6\text{-}(CF_3)Py)_3]Ag(C_3H_6)$. Yield: 100 mg (82%). ^{1}H NMR (400 MHz, $CDCl_3$, −40 °C): δ (ppm) 7.71 (d, J = 7.0 Hz, 3H, Py), 7.61 (t, J = 7.4 Hz, 3H, Py), 7.38 (d, J = 7.3 Hz, 3H, Py), 5.79 (m, 1H, C*H*, Prop), 4.72 (d, J = 16.6 Hz, 1H, C*H*H′, Prop), 4.56 (d, J = 9.0 Hz, 1H, CH*H*′, Prop), 1.65 (d, J = 5.6 Hz, 3H, CH_3, Prop), 0.54 (s, 3H, B–CH_3). ^{13}C{^{1}H} NMR (101 MHz, $CDCl_3$, −40 °C): δ (ppm) 187.2 (q, $^1J_{C-B}$ = 57.3 Hz, B-Py), 145.7 (q, $^2J_{C-F}$ = 31.7 Hz, *C*-CF_3), 135.3 (s, Py), 132.0 (s, Py), 122.0 (q, $^1J_{C-F}$ = 273.9 Hz, CF_3), 116.1 (s, Py), 95.2 (brs, Prop), 21.1 (s, Prop), 11.3 (br, B-CH_3).^{19}F NMR (471 MHz, $CDCl_3$, −40 °C): δ (ppm) = −67.82 (s). HR-MS [ESI, positive ion mode ESI-TOF]: m/z for $C_{19}H_{12}B_1F_9N_3Ag_1$ $[M - C_3H_6 + H]^+$ calcd 572.0109, found 572.0144.

$[MeB(6\text{-}(CF_3)Py)_3]Au(C_3H_6)$ (8). To a mixture of $[MeB(6\text{-}(CF_3)Py)_3]K$ (150 mg, 0.298 mmol, 1 equiv) and AuCl (76 mg, 0.328 mmol, 1.1 equiv) in a 50 mL Schlenk flask covered with aluminum foil, cold anhydrous dichloromethane (20 mL) was added, and then propylene (1 atm) was bubbled into the solution. The reaction mixture was stirred for 1 h at 0 °C and then for 30 min at room temperature. The reaction mixture was then cannula-filtered through a Celite-packed frit to remove KOTf and excess AuCl. The solution was concentrated under reduced pressure, and the compound was recrystallized in dichloromethane layered with hexane and kept at −20 °C to obtain colorless X-ray quality single crystals of $[MeB(6\text{-}(CF_3)Py)_3]Au(C_3H_6)$. Yield: 132 mg (63%). ^{1}H NMR (400 MHz, $CDCl_3$): δ (ppm) 8.31–8.20 (m, 1.18 H, Py^m, minor isomer), 7.87–7.79 (m, 1.33 H, Py^m, minor isomer), 7.74 (d, J = 7.5 Hz, 3H, Py), 7.68–7.62 (m, 1.33H + 3H, Py^m + Py), 7.44 (d, J = 7.6 Hz, 3H, Py),

Downloaded from http://pubs.acs.org/inocaj/article-pdf/65/25/14287/6524819/acs.inorgchem.6c01837.pdf by UNIV OF NORTH TEXAS user on 28 July 2026

https://doi.org/10.1021/acs.inorgchem.6c01837
Inorg. Chem. 2026, 65, 14287–14300

3.91 (br, 0.45H, C*H*, Prop^m, minor isomer) 3.72 (m, 1H, C*H*, Prop), 3.20 (br, 0.34H, C*H*H′, Prop^m, minor isomer), 3.00 (d, J = 8.4 Hz, 1H, C*H*H′, Prop), 2.55 (d, J = 13.5 Hz, 1H, CH*H*′, Prop), 2.49 (br, 0.30H, CH*H*′, Prop^m, minor isomer), 1.09 (d, J = 6.1 Hz, 1.84H, CH_3, Prop^m, minor isomer), 0.93 (d, J = 6.1 Hz, 3H, CH_3, Prop), 0.79 (s, 1.85H, B−CH_3^m, minor isomer), 0.52 (s, 3H, B−CH_3). ^{13}C{^{1}H} NMR (101 MHz, $CDCl_3$, −40 °C): δ (ppm): 187.6 (q, $^1J_{C-B}$ = 51.4 Hz, B-Py), 146.1 (q, $^2J_{C-F}$ = 33.1 Hz, *C*-CF$_3$), 137.6 (s, Py^m, minor isomer), 136.7 (s, Py^m, minor isomer), 135.4 (s, Py), 132.4 (s, Py), 122.1 (q, $^1J_{C-F}$ = 274.3 Hz, CF$_3$), 117.3 (s, Py), 116.8 (s, Py^m, minor isomer), 80.0 (s, Prop^m, minor isomer), 77.5 (s, Prop), 60.2 (s, Prop^m, minor isomer), 59.2 (s, Prop), 19.6 (s, Prop^m, minor isomer), 18.9 (s, Prop), 12.2 (q, $^1J_{C-B}$ = 45.3 Hz, B-CH$_3$). ^{19}F NMR (471 MHz, $CDCl_3$): δ (ppm) = −66.4 (s), −67.2 (s, minor isomer). HR-MS [ESI, positive ion mode ESI-TOF]: m/z for $C_{22}H_{18}B_1F_9N_3Au_1$ [M + H]$^+$ calcd 704.1194, found 704.1235. The [MeB(6-(CF$_3$)Py)$_3$]Au-(C$_3$H$_6$) can also be synthesized using AuCl(SMe$_2$) instead of AuCl in the above procedure.

[MeB(6-(CF$_3$)Py)$_3$]Cu (9). Solid [MeB(6-(CF$_3$)Py)$_3$]Cu(C$_3$H$_6$) was placed under reduced pressure at 40 °C for 1 h to remove propylene. The compound was recrystallized from THF at −20 °C to obtain colorless X-ray quality single crystals of [MeB(6-(CF$_3$)Py)$_3$]-Cu. ^{1}H NMR (400 MHz, DMSO-d_6): δ 7.81 (t, J = 7.5 Hz, 3H, Py), 7.65 (d, J = 7.4 Hz, 3H, Py), 7.56 (d, J = 7.5 Hz, 3H, Py), 0.47 (s, 3H, CH_3). ^{13}C{^{1}H} NMR (101 MHz, DMSO-d_6): δ (ppm) 185.9 (br, B-Py), 144.0 (q, $^2J_{C-F}$ = 32.0 Hz, *C*-CF$_3$), 135.8 (s, Py), 131.5 (s, Py), 121.9 (q, $^1J_{C-F}$ = 275 Hz, *C*F$_3$), 116.7 (s, Py), 10.5 (br, B-CH$_3$). ^{19}F NMR (376 MHz, DMSO-d_6): δ = −66.43 (s). Treatment of a concentrated dichloromethane solution of **9** with propylene led cleanly to **6**. Anal. Calcd $C_{19}H_{12}B_1Cu_1F_9N_3$: C, 43.25%; H, 2.29%; N, 7.96%. Found: C, 43.23%; H, 2.56%; N, 8.05%.

[MeB(6-(CF$_3$)Py)$_3$]Ag (10). Solid [MeB(6-(CF$_3$)Py)$_3$]Ag(C$_3$H$_6$) was placed under reduced pressure at room temperature for 10 min to remove propylene. The compound was recrystallized from either dichloromethane or THF at −20 °C to obtain colorless X-ray quality single crystals of [MeB(6-(CF$_3$)Py)$_3$]Ag. ^{1}H NMR (400 MHz, DMSO-d_6): δ 7.79 (t, J = 7.8 Hz, 3H, Py), 7.68 (d, J = 7.7 Hz, 3H, Py), 7.54 (dd, J = 7.7, 1.0 Hz, 3H, Py), 0.48 (s, 3H, CH_3).^{19}F NMR (376 MHz, DMSO-d_6): δ = −66.96 (s). ^{13}C{^{1}H} NMR (101 MHz, DMSO-d_6): δ (ppm) 186.6 (q, $^1J_{C-B}$ = 63.3 Hz, B-Py), 144.8 (q, $^2J_{C-F}$ = 31.6 Hz, *C*-CF$_3$, Py), 135.8 (s, Py), 131.3 (s, Py), 122.0 (q, $^1J_{C-F}$ = 274 Hz, *C*F$_3$), 116.2 (s, Py), 11.4 (d, $^1J_{C-B}$ = 33.3 Hz, B-CH$_3$). Treatment of a concentrated dichloromethane solution of **10** with propylene led cleanly to **7**. Anal. Calcd $C_{19}H_{12}B_1Ag_1F_9N_3$: C, 39.90%; H, 2.11%; N, 7.35%. Found: C, 40.07%; H, 2.18%; N, 7.36%.

X-ray Structure Determinations

A suitable crystal covered with a layer of hydrocarbon/Paratone-N oil was selected and mounted on a cryo loop and immediately placed in the low-temperature nitrogen stream. The X-ray intensity data were measured at 100(2) K (unless otherwise noted) on a Bruker Smart Apex II or Bruker D8 Quest equipped with an Oxford Cryosystems 700 series cooler, a graphite monochromator, and a Mo Kα fine-focus sealed tube (λ = 0.71073 Å). Intensity data were processed, and absorption corrections were applied using the Bruker Apex program suite. Initial atomic positions were located by SHELXT,[112] and the structures of the compounds were refined by the least-squares method using SHELXL[113] within Olex2 GUI.[114] Compounds [MeB(6-(CF$_3$)Py)$_3$]Cu(C$_3$H$_6$) (**6**) and [MeB(6-(CF$_3$)Py)$_3$]Ag(C$_3$H$_6$) (**7**) show positional disorder at the propylene moiety with % atomic occupancies of 60:40 and 72:28, respectively, and were modeled successfully. [MeB(6-(CF$_3$)Py)$_3$]Au(C$_3$H$_6$) (**8**) shows positional disorder at the gold and propylene moiety, with a % atomic occupancy of 58:42, and was modeled satisfactorily. Fluorine atoms in CF$_3$ groups of [MeB(6-(CF$_3$)Py)$_3$]Cu (**9**) show positional disorder, but it was modeled satisfactorily. All the hydrogen atoms in all complexes in this study were refined anisotropically. X-ray structural figures were generated using Olex2.

Computational Details

All computations were obtained by using relativistic DFT methods with the ADF code[115] [ADF 2024, SCM, Theoretical Chemistry, Vrije Universiteit, Amsterdam, The Netherlands, http://www.scm.com] utilizing an all-electron triple-z Slater basis set along with the double-polarization (STO-TZ2P) basis set, paired with the Becke−Perdew (BP86) functional[116] within the generalized gradient approximation (GGA). London dispersion corrections were incorporated through the pairwise Grimme (BP86-D3) method.[117] Geometry optimizations were conducted without any symmetry constraints using the analytical energy gradient method developed by Versluis and Ziegler,[118] with energy convergence criteria set at 10^{-4} Hartree, gradient convergence criteria at 10^{-4} Hartree/Å, and a radial convergence of 10^{-3} Å. Scalar relativistic effects were accounted for using the ZORA Hamiltonian.[119] The interaction energy is further broken down into several chemically significant components according to the Energy Decomposition Analysis (EDA) by Ziegler and Rauk,[120,121]

$$\Delta E_{int} = \Delta E_{Pauli} + \Delta E_{elstat} + \Delta E_{orb} + \Delta E_{disp}$$

where the ΔE_{Pauli} term involves electron repulsion between occupied orbitals from different fragments and ΔE_{elstat} and ΔE_{orb} are associated with the stabilizing electrostatic and covalent nature of the interaction, respectively. The contribution from dispersion interaction (ΔE_{disp}) is assessed using Grimme's pairwise correction (D3). Bonding analysis is provided in terms of bonding contributions to ΔE_{orb} using the Natural Orbitals for Chemical Valence extension of the EDA method (EDA-NOCV),[122] resulting in deformation densities that account for the individual in- and out-flow of charges related to the bonding pattern.

^{13}C NMR and ^{1}H NMR chemical shift calculations were obtained at the spin−orbit all-electron TZ2P/OPBE level by converting absolute shielding at the nucleus probe ($^C\sigma$ or $^H\sigma$, respectively) to chemical shifts by using tetramethylsilane as a reference with $^{C/H}\delta = {}^{C/H\text{-}TMS}\sigma - {}^{C/H}\sigma$, with $^{C\text{-}TMS}\sigma$= 193.2 and $^{H\text{-}TMS}\sigma$= 31.4 ppm.

Solid-State Adsorption Studies

A Micromeritics ASAP2020Plus surface area and porosity analyzer instrument was used for gas sorption measurements.

IAST calculations: Ideal adsorption solution theory (IAST) was used to calculate the C_3H_8/C_3H_6 selectivity for the ideal mixture compositions in materials at 298 K.[123,124] The dual-site Langmuir−Freundlich (DSLF) adsorption model is used to correlate the pure-component equilibrium data and further predict the adsorption of a mixture.

The adsorption selectivity for C_3H_8/C_3H_6 separation is defined by

$$S = \frac{q1/q2}{p1/p2}$$

where $q1$ and $q2$ are the molar loadings in the adsorbed phase in equilibrium with the bulk gas phase with partial pressures p1 and p2.

General Method for the Aziridination

A Schlenk flask was charged with alkene (0.4 mmol, 1 equiv), catalyst (5 mol %), 100 mg molecular sieves 4 Å, and anhydrous acetonitrile (2.0 mL) under a nitrogen atmosphere. When propylene was used as the substrate, propylene gas (1 atm) was bubbled through the solution for ca. 10 s. After the mixture was stirred for 5 min, solid PhI=NNs (0.6 mmol, 1.5 equiv) was directly added to the mixture in one portion under a positive flow of N_2. The mixture was stirred for 12 h at room temperature. It was filtered, the filtrate was collected, and the solvent was removed under reduced pressure. The NMR yield of the product was calculated using 1,3,5-trimethoxybenzene as an internal standard.

■ ASSOCIATED CONTENT

Supporting Information

The Supporting Information is available free of charge at https://pubs.acs.org/doi/10.1021/acs.inorgchem.6c01837.

Downloaded from http://pubs.acs.org/inocaj/article-pdf/65/25/14287/6524819/acs.inorgchem.6c01837.pdf by UNIV OF NORTH TEXAS user on 28 July 2026

https://doi.org/10.1021/acs.inorgchem.6c01837
Inorg. Chem. 2026, 65, 14287−14300

Twist angle between N_1−Ag−N_2 coordination plane and the C_{20}−Ag−C_{21} plane; possible isomers of the gold−propylene complex [MeB(6-(CF_3)Py)$_3$]Au(C_3H_6); NMR and Raman spectroscopic data, additional figures, summaries of data collection and refinement, adsorption studies, computational data, catalysis, and references; four possible isomers of the gold−propylene complex [MeB(6-(CF_3)Py)$_3$]Au(C_3H_6) (**8**); ^{1}H NMR,^{13}C{^{1}H} and ^{19}F NMR spectra of [MeB(6-(CF_3)Py)$_3$]Cu(C_3H_6) (**6**); Raman spectra of [MeB(6-(CF_3)Py)$_3$]Cu(C_3H_6) (top, **6**) and its propylene free [MeB(6-(CF_3)Py)$_3$]Cu (bottom, **9**); ^{1}H NMR,^{13}C{^{1}H} NMR, and ^{19}F NMR spectra of [MeB(6-(CF_3)Py)$_3$]Ag(C_3H_6) (**7**); Raman spectra and IR spectra of [MeB(6-(CF_3)Py)$_3$]Ag(C_3H_6) (top, **7**) and its propylene free [MeB(6-(CF_3)Py)$_3$]Ag (bottom, **10**); ^{1}H NMR, ^{13}C{^{1}H} NMR, and ^{19}F NMR spectra of [MeB(6-(CF_3)Py)$_3$]Au(C_3H_6) (**8**); ^{1}H NMR, ^{13}C{^{1}H} NMR, and ^{19}F NMR spectra of [MeB(6-(CF_3)Py)$_3$]Cu (**9**); ^{1}H NMR, ^{13}C{^{1}H} NMR, and ^{19}F NMR spectra of [MeB(6-(CF_3)Py)$_3$]Ag (**10**); crystal data and structure refinement and molecular structures for [MeB(6-(CF_3)Py)$_3$]Cu(C_3H_6) (**6**), [MeB(6-(CF_3)Py)$_3$]Ag(C_3H_6) (**7**), [MeB(6-(CF_3)Py)$_3$]Au(C_3H_6) (**8**), [MeB(6-(CF_3)Py)$_3$]Cu (**9**), and [MeB(6-(CF_3)Py)$_3$]Ag (**10**) (PDF)

Accession Codes

Deposition Numbers 2529682−2529686 contain the supplementary crystallographic data for this paper. These data can be obtained free of charge via the joint Cambridge Crystallographic Data Centre (CCDC) and Fachinformationszentrum Karlsruhe Access Structures service.

AUTHOR INFORMATION

Corresponding Authors

Alvaro Muñoz-Castro − *Facultad de Ingeniería, Universidad San Sebastián, Santiago 8420524, Chile;* orcid.org/0000-0001-5949-9449; Email: alvaro.munozc@uss.cl

Shengqian Ma − *University of North Texas, Denton, Texas 762031, United States;* orcid.org/0000-0002-1897-7069; Email: Shengqian.Ma@unt.edu

H. V. Rasika Dias − *The University of Texas at Arlington, Arlington, Texas 76019, United States;* orcid.org/0000-0002-2362-1331; Email: dias@uta.edu

Authors

Vo Quang Huy Phan − *The University of Texas at Arlington, Arlington, Texas 76019, United States;* orcid.org/0009-0004-3436-4168

Mukundam Vanga − *The University of Texas at Arlington, Arlington, Texas 76019, United States;* orcid.org/0000-0002-7822-4181

Sayan Maiti − *University of North Texas, Denton, Texas 762031, United States*

Complete contact information is available at: https://pubs.acs.org/10.1021/acs.inorgchem.6c01837

Notes

The authors declare no competing financial interest.

ACKNOWLEDGMENTS

This material was based on work supported by the University of Texas at Arlington, and in part supported by the U.S. Department of Agriculture, Agricultural Research Service, under agreement No. 58-2040-3-017, and the American Floral Endowment, an industry-funded nonprofit dedicated to sustaining and advancing floriculture research. Any opinions, findings, conclusions, or recommendations expressed in this publication are those of the author(s) and do not necessarily reflect the view of the U.S. Department of Agriculture. The USDA is an equal opportunity provider and employer. We thank Dr. Tony Pham at the University of South Florida for his assistance with the analysis of some of the isotherm data of the silver complex.

REFERENCES

(1) Shirzad, P.; Kantor, I. Toward sustainable propylene: A comparison of current and future production pathways. *Renewable and Sustainable Energy Transition* **2025**, *7*, No. 100099.

(2) Corma, A.; Corresa, E.; Mathieu, Y.; Sauvanaud, L.; Al-Bogami, S.; Al-Ghrami, M. S.; Bourane, A. Crude oil to chemicals: light olefins from crude oil. *Catal. Sci. Technol.* **2017**, *7* (1), 12−46.

(3) Lipshutz, B. H.; Yamamoto, Y. Introduction: Coinage Metals in Organic Synthesis. *Chem. Rev.* **2008**, *108* (8), 2793−2795.

(4) Haruta, M. Size- and support-dependency in the catalysis of gold. *Catal. Today* **1997**, *36* (1), 153−166.

(5) Okumura, M.; Fujitani, T.; Huang, J.; Ishida, T. A Career in Catalysis: Masatake Haruta. *ACS Catal.* **2015**, *5* (8), 4699−4707.

(6) Huang, J.; Akita, T.; Faye, J.; Fujitani, T.; Takei, T.; Haruta, M. Propene Epoxidation with Dioxygen Catalyzed by Gold Clusters. *Angew. Chem., Int. Ed.* **2009**, *48* (42), 7862−7866.

(7) Min, B. K.; Friend, C. M. Heterogeneous Gold-Based Catalysis for Green Chemistry: Low-Temperature CO Oxidation and Propene Oxidation. *Chem. Rev.* **2007**, *107* (6), 2709−2724.

(8) Teržan, J.; Huš, M.; Likozar, B.; Djinović, P. Propylene Epoxidation using Molecular Oxygen over Copper- and Silver-Based Catalysts: A Review. *ACS Catal.* **2020**, *10* (22), 13415−13436.

(9) Halder, A.; Warburton, R. E.; Sun, G.; Cheng, L.; Assary, R. S.; Seifert, S.; Homer, M.; Greeley, J.; Alexandrova, A. N.; Sautet, P.; Curtiss, L. A.; Vajda, S. Low-Temperature Direct Oxidation of Propane to Propylene Oxide Using Supported Subnanometer Cu Clusters. *ACS Catal.* **2025**, *15* (7), 5760−5769.

(10) Khatib, S. J.; Oyama, S. T. Direct Oxidation of Propylene to Propylene Oxide with Molecular Oxygen: A Review. *Catal. Rev.: Sci. Eng.* **2015**, *57* (3), 306−344.

(11) Qiu, Y.; Zhang, Y.; Zhang, R.; Huang, M.; Tan, K. B.; Zhan, G.; Fu, G.; Li, Q.; Huang, J. Internally hollow Cu_2O nanoframes with the abundance of {110} facets enhance direct propylene epoxidation. *Nat. Commun.* **2025**, *16* (1), 7802.

(12) Marimuthu, A.; Zhang, J.; Linic, S. Tuning Selectivity in Propylene Epoxidation by Plasmon Mediated Photo-Switching of Cu Oxidation State. *Science* **2013**, *339* (6127), 1590−1593.

(13) Gao, J.; Bahmanpour, A.; Kröcher, O.; Zakeeruddin, S. M.; Ren, D.; Grätzel, M. Electrochemical synthesis of propylene from carbon dioxide on copper nanocrystals. *Nat. Chem.* **2023**, *15* (5), 705−713.

(14) Li, C.; Zhang, H.; Liu, W.; Sheng, L.; Cheng, M.-J.; Xu, B.; Luo, G.; Lu, Q. Efficient conversion of propane in a microchannel reactor at ambient conditions. *Nat. Commun.* **2024**, *15* (1), 884.

(15) Newmeyer, E.-R.; Wang, Y.; Long, Z. A.; North, J. D.; Shi, Y.; Swearer, D. F. Plasmonic Charge Localization and C−H Activation at Single-Atom Sites in Dilute Copper Platinum Alloys. *J. Am. Chem. Soc.* **2025**, *147* (14), 11789−11799.

(16) Artsiusheuski, M. A.; Verel, R.; van Bokhoven, J. A.; Sushkevich, V. L. Selective Oxidative Dehydrogenation of Ethane and Propane over Copper-Containing Mordenite: Insights into Reaction Mechanism and Product Protection. *Angew. Chem., Int. Ed.* **2023**, *62* (44), No. e202309180.

Downloaded from http://pubs.acs.org/inocaj/article-pdf/65/25/14287/6524819/acs.inorgchem.6c01837.pdf by UNIV OF NORTH TEXAS user on 28 July 2026

(17) Artsiusheuski, M. A.; Guo, J.; Kulkarni, A. R.; van Bokhoven, J. A.; Sushkevich, V. L. Low-Temperature Nonoxidative Dehydrogenation of Short-Chain Alkanes over Copper(I) Mordenite via Chemical Looping. *J. Am. Chem. Soc.* **2025**, *147* (18), 15880−15889.
(18) Lashchinskaya, Z. N.; Gabrienko, A. A.; Stepanov, A. G. Propene transformation on Cu-modified ZSM-5 zeolite: Aromatization and oxidation. *Microporous Mesoporous Mater.* **2023**, *350*, No. 112448.
(19) Lashchinskaya, Z. N.; Gabrienko, A. A.; Stepanov, A. G. Mechanisms of Light Alkene Oligomerization on Metal-Modified Zeolites. *ACS Catal.* **2024**, *14* (7), 4984−4998.
(20) Yuan, B.-J.; Xu, S.-M.; Liu, X.; Li, A.-Z.; Wang, X.; Shi, Q.; Li, R.-P.; Zhang, C.; Zhao, X.; Zheng, J.; Li, B.-J.; Duan, H. Homogeneous silver catalyst for propylene electrooxidation to propylene glycol. *Nat. Commun.* **2025**, *16* (1), 10319.
(21) Song, W.; Perez Ferrandez, D. M.; van Haandel, L.; Liu, P.; Nijhuis, T. A.; Hensen, E. J. M. Selective Propylene Oxidation to Acrolein by Gold Dispersed on $MgCuCr_2O_4$ Spinel. *ACS Catal.* **2015**, *5* (2), 1100−1111.
(22) Zhang, Z.; Lee, S. D.; Widenhoefer, R. A. Intermolecular Hydroamination of Ethylene and 1-Alkenes with Cyclic Ureas Catalyzed by Achiral and Chiral Gold(I) Complexes. *J. Am. Chem. Soc.* **2009**, *131* (15), 5372−5373.
(23) Tian, Y.-J.; Deng, C.; Peng, Y.-L.; Zhang, X.; Zhang, Z.; Zaworotko, M. J. State of the art, challenges and prospects in metal−organic frameworks for the separation of binary propylene/propane mixtures. *Coord. Chem. Rev.* **2024**, *506*, No. 215697.
(24) Sholl, D. S.; Lively, R. P. Seven chemical separations to change the world. *Nature* **2016**, *532* (7600), 435−437.
(25) Liang, B.; Zhang, X.; Xie, Y.; Lin, R.-B.; Krishna, R.; Cui, H.; Li, Z.; Shi, Y.; Wu, H.; Zhou, W.; Chen, B. An Ultramicroporous Metal−Organic Framework for High Sieving Separation of Propylene from Propane. *J. Am. Chem. Soc.* **2020**, *142* (41), 17795−17801.
(26) Rege, S. U.; Yang, R. T. Propane/propylene separation by pressure swing adsorption: sorbent comparison and multiplicity of cyclic steady states. *Chem. Eng. Sci.* **2002**, *57* (7), 1139−1149.
(27) Safarik, D. J.; Eldridge, R. B. Olefin/Paraffin Separations by Reactive Absorption: A Review. *Ind. Eng. Chem. Res.* **1998**, *37* (7), 2571−2581.
(28) Geier, S. J.; Mason, J. A.; Bloch, E. D.; Queen, W. L.; Hudson, M. R.; Brown, C. M.; Long, J. R. Selective adsorption of ethylene over ethane and propylene over propane in the metal−organic frameworks M_2(dobdc) (M = Mg, Mn, Fe, Co, Ni, Zn). *Chem. Sci.* **2013**, *4* (5), 2054−2061.
(29) Noonikara-Poyil, A.; Cui, H.; Wang, B.; Shi, Y.; Chen, B.; Dias, H. V. R. Remarkably Selective Propylene−Propane Separation Using a Copper Scorpionate. *Small* **2023**, *19* (11), No. 2206984.
(30) Azhin, M.; Kaghazchi, T.; Rahmani, M. A review on olefin/paraffin separation using reversible chemical complexation technology. *J. Ind. Eng. Chem.* **2008**, *14* (5), 622−638.
(31) Choudary, N. V.; Kumar, P.; Bhat, T. S. G.; Cho, S. H.; Han, S. S.; Kim, J. N. Adsorption of Light Hydrocarbon Gases on Alkene-Selective Adsorbent. *Ind. Eng. Chem. Res.* **2002**, *41* (11), 2728−2734.
(32) Uchida, S.; Kawamoto, R.; Tagami, H.; Nakagawa, Y.; Mizuno, N. Highly Selective Sorption of Small Unsaturated Hydrocarbons by Nonporous Flexible Framework with Silver Ion. *J. Am. Chem. Soc.* **2008**, *130* (37), 12370−12376.
(33) Plaza, M. G.; Ferreira, A. F. P.; Santos, J. C.; Ribeiro, A. M.; Müller, U.; Trukhan, N.; Loureiro, J. M.; Rodrigues, A. E. Propane/propylene separation by adsorption using shaped copper trimesate MOF. *Micropor. Mesopor. Mater.* **2012**, *157*, 101−111.
(34) Wang, Y.; Peh, S. B.; Zhao, D. Alternatives to Cryogenic Distillation: Advanced Porous Materials in Adsorptive Light Olefin/Paraffin Separations. *Small* **2019**, *15* (25), No. 1900058.
(35) Cong, S.; Feng, X.; Guo, L.; Peng, D.; Wang, J.; Chen, J.; Zhang, Y.; Shen, X.; Yang, G. Rational Design of Mixed Matrix Membranes Modulated by Trisilver Complex for Efficient Propylene/Propane Separation. *Adv. Sci.* **2023**, *10* (10), No. 2206858.
(36) Kim, K. C.; Lee, C. Y.; Fairen-Jimenez, D.; Nguyen, S. T.; Hupp, J. T.; Snurr, R. Q. Computational Study of Propylene and Propane Binding in Metal−Organic Frameworks Containing Highly Exposed Cu^+ or Ag^+ Cations. *J. Phys. Chem. C* **2014**, *118* (17), 9086−9092.
(37) Wang, Y.-X.; Li, M.-H.; Cao, R.; Lei, M.; Sui, Z.-J.; Zhou, X.-G.; Chen, D.; Zhu, Y.-A. A machine-learning-assisted study of propylene adsorption behaviors on transition metals and alloys: Beyond the Dewar-Chatt-Duncanson model. *Chem. Catalysis* **2024**, *4* (2), No. 100875.
(38) Kim, J. H.; Min, B. R.; Kim, C. K.; Won, J.; Kang, Y. S. Spectroscopic Interpretation of Silver Ion Complexation with Propylene in Silver Polymer Electrolytes. *J. Phys. Chem. B* **2002**, *106* (10), 2786−2790.
(39) Park, S.; Morales-Collazo, O.; Freeman, B.; Brennecke, J. F. Ionic Liquid Stabilizes Olefin Facilitated Transport Membranes Against Reduction. *Angew. Chem., Int. Ed.* **2022**, *61* (25), No. e202202895.
(40) Song, Y.-Y.; Wang, G.-C. A DFT Study and Microkinetic Simulation of Propylene Partial Oxidation on CuO (111) and CuO (100) Surfaces. *J. Phys. Chem. C* **2016**, *120* (48), 27430−27442.
(41) Groom, C. R.; Bruno, I. J.; Lightfoot, M. P.; Ward, S. C. The Cambridge Structural Database. *Acta Crystallogr. Sect. B* **2016**, *72* (2), 171−179.
(42) Parasar, D.; Elashkar, A. H.; Yakovenko, A. A.; Jayaratna, N. B.; Edwards, B. L.; Telfer, S. G.; Dias, H. V. R.; Cowan, M. G. Overcoming Fundamental Limitations in Adsorbent Design: Alkene Adsorption by Non-porous Copper(I) Complexes. *Angew. Chem., Int. Ed.* **2020**, *59* (47), 21001−21006.
(43) Navarro, M.; Alférez, M. G.; de Sousa, M.; Miranda-Pizarro, J.; Campos, J. Dicoordinate Au(I)−Ethylene Complexes as Hydroamination Catalysts. *ACS Catal.* **2022**, *12* (7), 4227−4241.
(44) Mon, M.; Bruno, R.; Tiburcio, E.; Grau-Atienza, A.; Sepúlveda-Escribano, A.; Ramos-Fernandez, E. V.; Fuoco, A.; Esposito, E.; Monteleone, M.; Jansen, J. C.; Cano, J.; Ferrando-Soria, J.; Armentano, D.; Pardo, E. Efficient Gas Separation and Transport Mechanism in Rare Hemilabile Metal−Organic Framework. *Chem. Mater.* **2019**, *31* (15), 5856−5866.
(45) Dias, H. V. R.; Lovely, C. J. Carbonyl and Olefin Adducts of Coinage Metals Supported by Poly(pyrazolyl)borate and Poly(pyrazolyl)alkane Ligands and Silver Mediated Atom Transfer Reactions. *Chem. Rev.* **2008**, *108* (8), 3223−3238.
(46) Dias, H. V. R.; Wu, J. Structurally Characterized Coinage-Metal−Ethylene Complexes. *Eur. J. Inorg. Chem.* **2008**, *2008* (4), 509−522.
(47) Dias, H. V. R. Polyfluorinated ligand-supported organometallic complexes of copper, silver, and gold. *Pure Appl. Chem.* **2010**, *82* (3), 649−656.
(48) Watson, B. T.; Dias, H. V. R. Going for gold − the chemistry of structurally authenticated gold(i)−ethylene complexes. *Chem. Commun.* **2024**, *60* (37), 4872−4889.
(49) Watson, B. T.; Vanga, M.; Noonikara-Poyil, A.; Muñoz-Castro, A.; Dias, H. V. R. Copper(I), Silver(I), and Gold(I) Ethylene Complexes of Fluorinated and Boron-Methylated Bis- and Tris(pyridyl)borate Chelators. *Inorg. Chem.* **2023**, *62* (4), 1636−1648.
(50) Lavoie, K. D.; Frauhiger, B. E.; White, P. S.; Templeton, J. L. Cationic Pt(IV) Tp' carbenes. *J. Organomet. Chem.* **2015**, *793*, 182−191.
(51) De Renzi, A.; Di Blasio, B.; Saporito, A.; Scalone, M.; Vitagliano, A. Synthesis, structure, and stereochemistry of five-coordinate platinum(II)-olefin complexes with a chiral diamine. *Inorg. Chem.* **1980**, *19* (4), 960−966.
(52) Chadwick, F. M.; McKay, A. I.; Martinez-Martinez, A. J.; Rees, N. H.; Krämer, T.; Macgregor, S. A.; Weller, A. S. Solid-state molecular organometallic chemistry. Single-crystal to single-crystal reactivity and catalysis with light hydrocarbon substrates. *Chem. Sci.* **2017**, *8* (9), 6014−6029.
(53) Findlater, M.; Cartwright-Sykes, A.; White, P. S.; Schauer, C. K.; Brookhart, M. Role of Coordination Geometry in Dictating the

Downloaded from http://pubs.acs.org/inocaj/article-pdf/65/25/14287/6524819/acs.inorgchem.6c01837.pdf by UNIV OF NORTH TEXAS user on 28 July 2026

Barrier to Hydride Migration in d^6 Square-Pyramidal Iridium and Rhodium Pincer Complexes. *J. Am. Chem. Soc.* **2011**, *133* (31), 12274−12284.
(54) Poole, A. D.; Gibson, V. C.; Clegg, W. Half-sandwich niobium(III) nitrene (Imido) complexes containing carbonyl, alkene and acetylene ligands. *J. Chem. Soc., Chem. Commun.* **1992**, *3*, 237−239.
(55) Cordero, B.; Gómez, V.; Platero-Prats, A. E.; Revés, M.; Echeverría, J.; Cremades, E.; Barragán, F.; Alvarez, S. Covalent radii revisited. *Dalton Trans.* **2008**, *21*, 2832−2838.
(56) Reisinger, A.; Trapp, N.; Knapp, C.; Himmel, D.; Breher, F.; Rüegger, H.; Krossing, I. Silver−Ethene Complexes $[Ag(\eta^2\text{-}C_2H_4)_n][Al(OR^F)_4]$ with n = 1, 2, 3 (R^F=Fluorine-Substituted Group). *Chem.−Eur. J.* **2009**, *15* (37), 9505−9520.
(57) Lide, D. R., Jr.; Christensen, D. Molecular Structure of Propylene. *J. Chem. Phys.* **1961**, *35* (4), 1374−1378.
(58) Nyholm, R. S. Proceedings of the Chemical Society. August 1961. *Proc. Chem. Soc.* **1961**, 273−320.
(59) Elschenbroich, C. *Organometallics*. 3rd ed.; Wiley-VCH: Weinheim, 2006; p 1−804.
(60) Hahn, C.; Morvillo, P.; Herdtweck, E.; Vitagliano, A. Coordination of Alkenes at a Highly Electrophilic Site. New Dicationic Platinum(II) Complexes: Synthesis, Structure, and Reactions with Nucleophiles. *Organometallics* **2002**, *21* (9), 1807−1818.
(61) de Klerk-Engels, B.; Delis, J. G. P.; Vrieze, K.; Goubitz, K.; Fraanje, J. Synthesis of Cyclopentadienyl(1,4-diisopropyl-1,3-diazabutadiene)(L)ruthenium Trifluoromethanesulfonate (L = Alkene, Alkyne, CO, Pyridine, PPh_3). X-ray Structure of $[(\eta^5\text{-}C_5H_5)Ru(^i\text{Pr-DAB})(\eta^2\text{-propene})][CF_3SO_3]$. *Organometallics* **1994**, *13* (8), 3269−3278.
(62) Oguadinma, P. O.; Schaper, F. π Back-Bonding in Dibenzyl-β-diketiminato Copper Olefin Complexes. *Organometallics* **2009**, *28* (23), 6721−6731.
(63) Alvarez, S. A cartography of the van der Waals territories. *Dalton Trans.* **2013**, *42* (24), 8617−8636.
(64) Dias, H. V. R.; Lu, H.-L.; Ratcliff, R. E.; Bott, S. G. Synthesis and Structure of [Hydridotris(3,5-bis(trifluoromethyl)pyrazolyl)-borato]potassium. *Inorg. Chem.* **1995**, *34* (8), 1975−1976.
(65) Carrier, S. M.; Ruggiero, C. E.; Houser, R. P.; Tolman, W. B. Synthesis, structural characterization, and electrochemical behavior of copper(I) complexes of sterically hindered tris(3-tert-butyl- and 3,5-diphenylpyrazolyl)hydroborate ligands. *Inorg. Chem.* **1993**, *32* (22), 4889−4899.
(66) Rodríguez, M. R.; Molina, F.; Díaz-Requejo, M. M.; Pérez, P. J. Copper and Silver Trispyrazolylborate-Phosphinoazide Complexes: Synthesis, Characterization, and Nitrene Generation. *Inorg. Chem.* **2025**, *64* (1), 151−157.
(67) Urbano, J.; Braga, A. A. C.; Maseras, F.; Álvarez, E.; Díaz-Requejo, M. M.; Pérez, P. J. The Mechanism of the Catalytic Functionalization of Haloalkanes by Carbene Insertion: An Experimental and Theoretical Study. *Organometallics* **2009**, *28* (20), 5968−5981.
(68) Humphrey, E. R.; Reeves, Z.; Jeffery, J. C.; McCleverty, J. A.; Ward, M. D. A long-standing structural puzzle resolved: the crystal structure of $[Ag_2(Tp^{Me,Me})_2]$ [where $Tp^{Me,Me}$ is hydrotris(3,5-dimethyl-pyrazolyl)borate]. *Polyhedron* **1999**, *18* (8), 1335−1338.
(69) Hu, Z.; Williams, R. D.; Tran, D.; Spiro, T. G.; Gorun, S. M. Re-engineering Enzyme-Model Active Sites: Reversible Binding of Dioxygen at Ambient Conditions by a Bioinspired Copper Complex. *J. Am. Chem. Soc.* **2000**, *122* (14), 3556−3557.
(70) Mealli, C.; Arcus, C. S.; Wilkinson, J. L.; Marks, T. J.; Ibers, J. A. Structural studies of copper(I) binding by hydrotris(1-pyrazolyl)-borate and hydrotris(3,5-dimethyl-1-pyrazolyl)borate in the solid state and in solution. *J. Am. Chem. Soc.* **1976**, *98* (3), 711−718.
(71) Kiani, S.; Long, J. R.; Stavropoulos, P. Evidence for Cu···H interactions in dinuclear Cu(I) complexes of hindered hydrotris (pyrazolyl) borate ligands. *Inorg. Chim. Acta* **1997**, *263* (1), 357−366.
(72) Yoon, K.; Parkin, G. Tris(3-t-butyl-5-methylpyrazolyl)-hydroborato derivatives of copper and thallium: The structural influence of a 5-methyl substituent. *Polyhedron* **1995**, *14* (6), 811−821.
(73) Augenstein, T.; Dorner, F.; Reiter, K.; Wagner, H. E.; Garnier, D.; Klopper, W.; Breher, F. A Boron-Fluorinated Tris(pyrazolyl)-borate Ligand (FTp*) and Its Mono- and Dinuclear Copper Complexes $[Cu(FTp^*)_2]$ and $[Cu_2(FTp^*)_2]$: Synthesis, Structures, and DFT Calculations. *Chem.−Eur. J.* **2016**, *22* (23), 7935−7943.
(74) Noonikara-Poyil, A.; Cui, H.; Yakovenko, A. A.; Stephens, P. W.; Lin, R.-B.; Wang, B.; Chen, B.; Dias, H. V. R. A Molecular Compound for Highly Selective Purification of Ethylene. *Angew. Chem., Int. Ed.* **2021**, *60* (52), 27184−27188.
(75) Dias, H. V. R.; Wu, J.; Wang, X.; Rangan, K. Structural Variations of Silver Ethylene Complexes Supported by Boron-Protected Fluorinated Scorpionates and the Isolation of a Ligand-Directed Silver Helix. *Inorg. Chem.* **2007**, *46* (6), 1960−1962.
(76) Adams, H.; Batten, S. R.; Davies, G. M.; Duriska, M. B.; Jeffery, J. C.; Jensen, P.; Lu, J.; Motson, G. R.; Coles, S. J.; Hursthouse, M. B.; Ward, M. D. New bis-, tris- and tetrakis(pyrazolyl)borate ligands with 3-pyridyl and 4-pyridyl substituents: synthesis and coordination chemistry. *Dalton Trans.* **2005**, *11*, 1910−1923.
(77) McSkimming, A. Flash Communication: On "Ag[$BArF_4$]" and an Expedient Synthesis of $[Ag(C_6H_6)_3][BArF_4]$. *Organometallics* **2025**, *44* (15), 1630−1632.
(78) Vanga, M.; Phan, V. Q. H.; Wu, J.; Muñoz-Castro, A.; Dias, H. V. R. Thallium(I) Complexes of Tris(pyridyl)borates and a Comparison to Their Pyrazolyl Analogues. *Inorg. Chem.* **2023**, *62* (45), 18563−18572.
(79) Ray, M.; Hammes, B. S.; Yap, G. P. A.; Rheingold, A. L.; Borovik, A. S. Structure and Physical Properties of Trigonal Monopyramidal Iron(II), Cobalt(II), Nickel(II), and Zinc(II) Complexes. *Inorg. Chem.* **1998**, *37* (7), 1527−1532.
(80) Searls, C. E.; Kleespies, S. T.; Eppright, M. L.; Schwartz, S. C.; Yap, G. P. A.; Scarrow, R. C. Trigonal Bi- and Monopyramidal Cobalt(II) Complexes of a Novel Guanidine-Based Tripodal Ligand. *Inorg. Chem.* **2010**, *49* (24), 11261−11263.
(81) Cummins, C. C.; Lee, J.; Schrock, R. R.; Davis, W. D. Trigonal-Monopyramidal M^{III} Complexes of the Type $[M(N_3N)]$ (M = Ti, V, Cr, Mn, Fe; $N_3N = [(tBuMe_2Si)CH_2CH_2]_3N$). *Angew. Chem., Int. Ed. Engl.* **1992**, *31* (11), 1501−1503.
(82) Hammond, M.; Rauch, M.; Parkin, G. Synthesis, Structure, and Reactivity of a Terminal Cadmium Hydride Compound, [κ^3-TismPr^{i}Benz]CdH. *J. Am. Chem. Soc.* **2021**, *143* (28), 10553−10559.
(83) Stenlid, J. H.; Brinck, T. Extending the σ-Hole Concept to Metals: An Electrostatic Interpretation of the Effects of Nanostructure in Gold and Platinum Catalysis. *J. Am. Chem. Soc.* **2017**, *139* (32), 11012−11015.
(84) Clark, T. σ-Holes. *WIREs Comput. Mol. Sci.* **2013**, *3* (1), 13−20.
(85) Walker, M. G.; Mendez, C. G.; Ho, P. S. Non-classical Non-covalent σ-Hole Interactions in Protein Structure and Function: Concepts for Potential Protein Engineering Applications. *Chem.−Asian J.* **2023**, *18* (7), No. e202300026.
(86) Noonikara-Poyil, A.; Muñoz-Castro, A.; Boretskyi, A.; Mykhailiuk, P. K.; Dias, H. V. R. When SF_5 outplays CF_3: effects of pentafluorosulfanyl decorated scorpionates on copper. *Chem. Sci.* **2021**, *12* (43), 14618−14623.
(87) Jiang, S.; Li, J.; Feng, M.; Chen, R.; Guo, L.; Xu, Q.; Chen, L.; Shen, F.; Zhang, Z.; Yang, Y.; Ren, Q.; Yang, Q.; Bao, Z. Hydrophobic paraffin-selective pillared-layer MOFs for olefin purification. *J. Mater. Chem. A* **2022**, *10* (45), 24127−24136.
(88) Verma, G.; Roknuzzaman, R.; Tan, K.; Kapoor, M.; Pham, T.; Maiti, S.; Phipps, J.; Kumar, S.; AlShahrani, T.; Ma, S. Highly Robust Zr-MOF Platform Featuring Aromatic-Rich Cores for Efficient Paraffin/Olefin Separation. *Energy Fuels* **2025**, *39* (23), 11308−11315.
(89) Wang, Y.; Li, T.; Li, L.; Lin, R.-B.; Jia, X.; Chang, Z.; Wen, H.-M.; Chen, X.-M.; Li, J. Construction of Fluorinated Propane-Trap in

Downloaded from http://pubs.acs.org/inocaj/article-pdf/65/25/14287/6524819/acs.inorgchem.6c01837.pdf by UNIV OF NORTH TEXAS user on 28 July 2026

https://doi.org/10.1021/acs.inorgchem.6c01837
Inorg. Chem. 2026, 65, 14287−14300

Metal−Organic Frameworks for Record Polymer-Grade Propylene Production under High Humidity Conditions. *Adv. Mater.* **2023**, *35* (14), No. 2207955.
(90) McQuade, J.; Jäkle, F. Tris(pyridyl)borates: an emergent class of versatile and robust polydentate ligands for catalysis and materials applications. *Dalton Trans.* **2023**, *52* (30), 10278−10285.
(91) Noonikara-Poyil, A.; Phan, V. Q. H.; Vanga, M.; Boretskyi, A.; Mykhailiuk, P.; Dias, H. V. R. Fluorinated B-phenylated scorpionates as tunable platforms for stabilizing thallium(i) and silver(i)−ethylene complexes. *Dalton Trans.* **2026**, *55* (1), 152−164.
(92) Phan, V. Q. H.; Adhikary, S. D.; Jeon, J.; Dias, H. V. R. Regio- and Diastereoselective C−C Silylation of Cyclopropyl Acetates Harnessing Fluorinated Poly(pyridyl)Borate Rhodium Catalysts. *Chem.−Eur. J.* **2026**, No. e03217.
(93) Pal, S.; Zavalij, P. Y.; Vedernikov, A. N. Oxidative C(sp^3)−H bond cleavage, C−C and C = C coupling at a boron center with O_2 as the oxidant mediated by platinum(II). *Chem. Commun.* **2014**, *50* (40), 5376−5378.
(94) Khaskin, E.; Zavalij, P. Y.; Vedernikov, A. N. Oxidatively Induced Methyl Transfer from Boron to Platinum in Dimethyldi(2-pyridyl)boratoplatinum Complexes. *Angew. Chem., Int. Ed.* **2007**, *46* (33), 6309−6312.
(95) Pal, S.; Zavalij, P. Y.; Vedernikov, A. N. Concurrent B-to-Pt Methyl Migration and B-Center Retention in Aerobic Oxidation of Methylborato Platinum(II) Complexes. *Organometallics* **2015**, *34* (20), 5183−5190.
(96) Fujiwara, Y.; Takayama, T.; Nakazawa, J.; Okamura, M.; Hikichi, S. Development of a novel scorpionate ligand with 6-methylpyridine and comparison of the structural and electronic properties of nickel(II) complexes with related tris(azolyl)borates. *Dalton Trans.* **2022**, *51* (27), 10338−10342.
(97) Qian, J.; Comito, R. J. Ethylene Polymerization with Thermally Robust Vanadium(III) Tris(2-pyridyl)borate Complexes. *Organometallics* **2023**, *42* (12), 1254−1258.
(98) Qian, J.; Comito, R. J. A Robust Vanadium(V) Tris(2-pyridyl)borate Catalyst for Long-Lived High-Temperature Ethylene Polymerization. *Organometallics* **2021**, *40* (12), 1817−1821.
(99) Qian, J.; Comito, R. J. Site-Isolated Main-Group Tris(2-pyridyl)borate Complexes by Pyridine Substitution and Their Ring-Opening Polymerization Catalysis. *Inorg. Chem.* **2022**, *61* (28), 10852−10862.
(100) Conley, B. L.; Guess, D.; Williams, T. J. A Robust, Air-Stable, Reusable Ruthenium Catalyst for Dehydrogenation of Ammonia Borane. *J. Am. Chem. Soc.* **2011**, *133* (36), 14212−14215.
(101) Sweeney, J. B. Aziridines: epoxides' ugly cousins? *Chem. Soc. Rev.* **2002**, *31* (5), 247−258.
(102) Thakur, V. V.; Sudalai, A. N-Bromoamides as versatile catalysts for aziridination of olefins using chloramine-T. *Tetrahedron Lett.* **2003**, *44* (5), 989−992.
(103) Tan, H.; Thai, P.; Sengupta, U.; Deavenport, I. R.; Kucifer, C. M.; Powers, D. C. Metal-Free Aziridination of Unactivated Olefins via Transient N-Pyridinium Iminoiodinanes. *JACS Au* **2024**, *4* (11), 4187−4193.
(104) Kiyokawa, K.; Kosaka, T.; Minakata, S. Metal-Free Aziridination of Styrene Derivatives with Iminoiodinane Catalyzed by a Combination of Iodine and Ammonium Iodide. *Org. Lett.* **2013**, *15* (18), 4858−4861.
(105) Yap, G. P. A.; Jove, F.; Urbano, J.; Alvarez, E.; Trofimenko, S.; Díaz-Requejo, M. M.; Pérez, P. J. Unusual Polybrominated Polypyrazolylborates and Their Copper(I) Complexes: Synthesis, Characterization, and Catalytic Activity. *Inorg. Chem.* **2007**, *46* (3), 780−787.
(106) Evans, D. A.; Bilodeau, M. T.; Faul, M. M. Development of the Copper-Catalyzed Olefin Aziridination Reaction. *J. Am. Chem. Soc.* **1994**, *116* (7), 2742−2753.
(107) Pérez, J.; Morales, D.; García-Escudero, L. A.; Martínez-García, H.; Miguel, D.; Bernad, P. Synthesis of new copper(I) complexes with tris(2-pyridyl) ligands. Applications to carbene and nitrene transfer reactions. *Dalton Trans.* **2009**, *2*, 375−382.
(108) Mairena, M. A.; Díaz-Requejo, M. M.; Belderraín, T. R.; Nicasio, M. C.; Trofimenko, S.; Pérez, P. J. Copper-Homoscorpionate Complexes as Very Active Catalysts for the Olefin Aziridination Reaction. *Organometallics* **2004**, *23* (2), 253−256.
(109) Dias, H. V. R.; Lu, H.-L.; Kim, H.-J.; Polach, S. A.; Goh, T. K. H. H.; Browning, R. G.; Lovely, C. J. Copper(I) Ethylene Adducts and Aziridination Catalysts Based on Fluorinated Tris(pyrazolyl)-borates $[HB(3\text{-}(CF_3),5\text{-}(R)Pz)_3]^-$ (where R = CF_3, C_6H_5, H; Pz = pyrazolyl). *Organometallics* **2002**, *21* (7), 1466−1473.
(110) Medina-Mercado, I.; Colin-Molina, A.; Barquera-Lozada, J. E.; Rodríguez-Molina, B.; Porcel, S. Gold-Catalyzed Ascorbic Acid-Induced Arylative Carbocyclization of Alkynes with Aryldiazonium Tetrafluoroborates. *ACS Catal.* **2021**, *11* (15), 8968−8977.
(111) Passia, M. T.; Bormann, N.; Ward, J. S.; Rissanen, K.; Bolm, C. Synthesis of N-Monosubstituted Sulfondiimines by Metal-free Iminations of Sulfilimium Salts. *Angew. Chem., Int. Ed.* **2023**, *62* (29), No. e202305703.
(112) Sheldrick, G. SHELXT - Integrated space-group and crystal-structure determination. *Acta Crystallogr. Sect. A: Found. Adv.* **2015**, *71* (1), 3−8.
(113) Sheldrick, G. Crystal structure refinement with SHELXL. *Acta Crystallogr. Sect. C: Struct. Chem.* **2015**, *71* (1), 3−8.
(114) Dolomanov, O. V.; Bourhis, L. J.; Gildea, R. J.; Howard, J. A. K.; Puschmann, H. OLEX2: a complete structure solution, refinement and analysis program. *J. Appl. Crystallogr.* **2009**, *42* (2), 339−341.
(115) ADF 2024, S. *Theoretical Chemistry*; Vrije Universiteit: Amsterdam, The Netherlands, http://www.scm.com.
(116) Becke, A. D. Density-functional exchange-energy approximation with correct asymptotic behavior. *Phys. Rev. A* **1988**, *38* (6), 3098−3100.
(117) Grimme, S. Density functional theory with London dispersion corrections. *WIREs Comput. Mol. Sci.* **2011**, *1* (2), 211−228.
(118) Versluis, L.; Ziegler, T. The determination of molecular structures by density functional theory. The evaluation of analytical energy gradients by numerical integration. *J. Chem. Phys.* **1988**, *88* (1), 322−328.
(119) van Lenthe, E.; Baerends, E. J.; Snijders, J. G. Relativistic total energy using regular approximations. *J. Chem. Phys.* **1994**, *101* (11), 9783−9792.
(120) Ziegler, T.; Rauk, A. On the calculation of bonding energies by the Hartree Fock Slater method. *Theor. Chim. Acta.* **1977**, *46* (1), 1−10.
(121) Hopffgarten, M. v.; Frenking, G. Energy decomposition analysis. *WIREs Comput. Mol. Sci.* **2012**, *2* (1), 43−62.
(122) Mitoraj, M. P.; Michalak, A.; Ziegler, T. A Combined Charge and Energy Decomposition Scheme for Bond Analysis. *J. Chem. Theory Comput.* **2009**, *5* (4), 962−975.
(123) Myers, A. L.; Prausnitz, J. M. Thermodynamics of mixed-gas adsorption. *AIChE J.* **1965**, *11* (1), 121−127.
(124) Lin, R.-B.; Li, L.; Zhou, H.-L.; Wu, H.; He, C.; Li, S.; Krishna, R.; Li, J.; Zhou, W.; Chen, B. Molecular sieving of ethylene from ethane using a rigid metal−organic framework. *Nat. Mater.* **2018**, *17* (12), 1128−1133.

Downloaded from http://pubs.acs.org/inocaj/article-pdf/65/25/14287/6524819/acs.inorgchem.6c01837.pdf by UNIV OF NORTH TEXAS user on 28 July 2026

https://doi.org/10.1021/acs.inorgchem.6c01837
Inorg. Chem. 2026, 65, 14287−14300